APL Photonics

PERSPECTIVE | AUGUST 02 2023

Present and future of terahertz integrated photonic devices

Shima Rajabali ; Ileana-Cristina Benea-Chelmus

APL Photonics 8, 080901 (2023)
https://doi.org/10.1063/5.0146912

Present and future of terahertz integrated photonic devices

Cite as: APL Photon. 8, 080901 (2023); doi: 10.1063/5.0146912
Submitted: 17 February 2023 • Accepted: 10 July 2023 •
Published Online: 2 August 2023

Shima Rajabali[1] and Ileana-Cristina Benea-Chelmus[1,2,a)]

AFFILIATIONS

[1] Hybrid Photonics Laboratory, EPF Lausanne, Lausanne, Switzerland
[2] Harvard John A. Paulson School of Engineering and Applied Sciences, Harvard University, Cambridge, Massachusetts 02138, USA

[a)] **Author to whom correspondence should be addressed:** cristina.benea@epfl.ch

ABSTRACT

Photonic integrated circuits have benefited many fields in the natural sciences. Their nanoscale patterning has led to the discovery of novel sources and detectors from ultraviolet to microwaves. Yet terahertz technologies have so far leveraged surprisingly little of the design and material freedom provided by photonic integrated circuits. Despite photoconduction—the process in which light is absorbed above the bandgap of a semiconductor to generate free carriers—and nonlinear up- and down-conversion being by far the two most widespread approaches to generate and detect terahertz waves, so far, terahertz technologies have been mostly employed in bulk. In this perspective, we discuss the current state-of-the-art, challenges, and perspectives for hybrid optical-terahertz photonic chips. We focus, in particular, on $\chi^{(2)}$ and $\chi^{(3)}$ nonlinear waveguides and waveguide-integrated photoconductive devices. We highlight opportunities in the micro- and macroscale design of waveguide geometries and printed antennas for the optimization of emission and detection efficiencies of terahertz waves. Realizing complex functionalities for terahertz photonics on a single chip may come into reach by integration and miniaturization compatible with telecom and fiber technologies.

I. INTRODUCTION

Traditional terahertz systems, dealing with radiation from 300 GHz to 10 THz, are bulky, in stark contrast with microwave systems (a few tens or hundreds of gigahertz). This stems from the periphery (equipment and cabling) of both detectors and emitters rather than the active core. Their bulkiness represents a clear hindrance to their broad deployment in the strategic areas shown in Fig. 1, where they would otherwise bring important advantages. For example, terahertz communication systems[1] are supposed to transport more information per second compared to microwaves, but terahertz transmitters and receivers need to have a low footprint, be cheap, and be mass-manufacturable. In sensing, terahertz systems have the ability to image through optically opaque media without inducing ionization, in clear contrast to x-rays, but they need to be high-speed, high-resolution, and turn-key. In manufacturing, terahertz imaging[2] can complement visible imaging and reveal both the compositional and morphological properties of products,[3,4] but it needs to contain a large number of pixels of small dimensions (<100 μm). In environmental monitoring and medical applications,[5] terahertz waves can detect water *in vivo*, e.g., in plants or human tissue, since the water has strong resonances in the terahertz, but they should be compatible with small samples that have sub-100 μm thicknesses. In quantum sciences, terahertz waves are key to selectively accessing otherwise inaccessible matter excitations like roto-vibrational modes, electronic transitions, e.g., in two-dimensional electron gases, or transitions between Rydberg states,[6–8] but terahertz sources need to be seamlessly integrated with these systems, which have extremely low dimensionality. In astronomy, terahertz local oscillators are suited to detect oxygen in the universe,[9,10] but they should be light enough to be mounted on satellites or planes orbiting the earth at altitudes where atmospheric absorption does not weaken signals from outer space. Finally, also in wearables, in the context of the internet of things, the requirements for compactness and low cost are extremely stringent.

Instead, at optical frequencies, miniaturization has been a powerful resource. Integrated platforms are ubiquitous for photonic

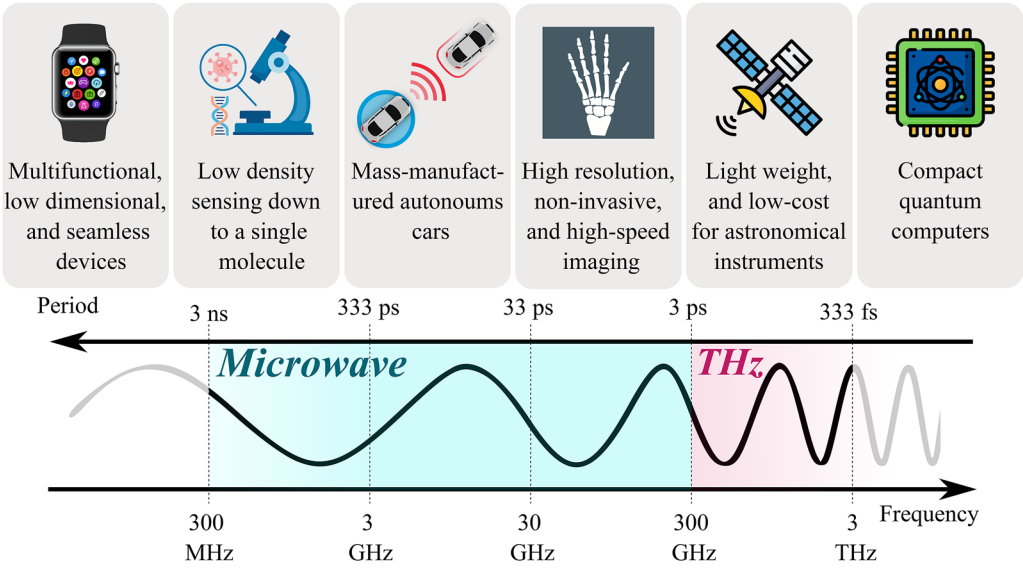

FIG. 1. Millimeter wave and terahertz research: motivations and applications. Miniaturization and integration can provide opportunities for high-speed data transmission with small-footprint transceivers in telecommunication and autonomous cars, compact wearables, low-density sensing, seamlessly integrated quantum devices, low-weight and low-cost astronomical instruments, and single-shot and non-invasive imaging operating in the millimeter wave and terahertz regions of the electromagnetic spectrum. Sources: Refs. 11–16.

applications, e.g., in frequency combs,[17–19] computing,[20,21] sensing,[22,23] and quantum science.[24–26] Adding microwave and terahertz to the photonic palette further enriches the variety of demonstrated components. On the source side, narrowband high-frequency waves are a crucial requirement when exploiting the coherent, parametric driving of sum- and difference frequency generation, Rabi oscillations, or electrical injection locking. Examples of photonic devices that rely on this principle are modulators,[27,28] electro-optic frequency combs,[19,29,30] photonic molecules,[31–33] driven light–matter systems,[34] the distribution and locking of time, and atomic clocks.[35,36] On the contrary, broadband pulses are applied to switch elementary excitations on picosecond time scales. Examples thereof include the application of π-pulses to excite a quantum system into a superposition or a well-defined state.[37] On the detector side, the metrology of microwaves downstream from a photonic chip is highly relevant. Examples are stabilization and locking schemes that require an in-loop characterization of noise (such as timing jitter and repetition rate drift) and then its control in real-time. So far, the bulk of applications have been restricted to microwaves, not yet reaching terahertz. For example, to the best of our knowledge, electro-optic frequency combs have been demonstrated up to several tens of gigahertz.[38] To reach higher repetition rates, demonstrations have resorted to modulation-induced instabilities to force pulse generation at the second and third harmonics of the fundamental repetition rate.[39]

Given the rich palette of components that rely on optical-electronic interplay, it is worthwhile asking the question, Where do these microwave signals come from, and how are they detected? Currently, microwave and terahertz signals stem, most of the time, from an external instrument. This requires them to be guided along coaxial cables and then applied to miniaturized photonic chips via RF probes. When guiding along cables becomes utterly impractical—as is the case in the terahertz, where standard cables are lossy, rigid, hollow, and very thin—the only alternative left is to broadcast the wave into free space and then recollect it by, e.g., horns or printed antennas at the receiver. However, in this case, water absorption may strongly attenuate the terahertz signal, depending on its frequency.[40] Once they arrive at the receiver, the waves may be sent further to monitoring electronics such as a vector network analyzer. This modular approach has important advantages. It allows us to combine state-of-the-art all-electronic equipment with microwave chips that have low dimensionality. It comes at the price of high insertion losses, which significantly worsen at higher frequencies, and absorption losses in free space. Furthermore, the power output of all-electronic sources is drastically decreasing toward the terahertz (the typical cutoff features a 20 dB/decade slope, characteristic of RC-type low-pass filters).

More recently, the success of platforms like silicon-on-insulator, hybrid silicon-organic, silicon nitride, diamond, or lithium niobate has inoculated the idea that these platforms would be sufficiently viable for the generation and detection of terahertz waves. While "RF photonics" is by now an established term that represents the research that utilizes optical carriers to generate and detect microwaves, "THz photonics" is similarly in its beginnings. This question has been pursued with a triple focus: first, the hallmark properties of photonics such as ultra-low-noise could be translated to the generation of terahertz waves by exploring coherent processes; second, miniaturization could enable more efficient devices; and, finally, making the need for cables obsolete by generating terahertz waves directly on the chip, right next to the optical components that utilize them. The aim would be to reduce propagation losses by keeping distances short and increasing end-to-end injection efficiency.

As a result, the focus started increasing on various photonic technologies, in particular those that exhibit the second and third-order nonlinearities of $\chi^{(2)}$ and $\chi^{(3)}$ or semiconductors, e.g., indium gallium arsenide, as a viable path to realize appreciable terahertz components inside miniaturized waveguides. These would thereby cohabit with photonics. The goal of the current perspective is threefold: 1. to sketch—by virtue of contrast—the principles of state-of-the-art terahertz generation and detection in $\chi^{(2)}$, $\chi^{(3)}$ and semiconducting photonic integrated circuits (PICs); 2. to argue that the potential success of miniaturization of terahertz-optical chips strictly relies on a few fundamental properties of these employed platforms: losses, dispersion, and nonlinearities; and 3. to outline the most pressing questions ahead. Our central hypothesis is that concerted efforts are necessary along the following lines to make the transition from bulk to on-chip terahertz photonics a possible and worthwhile enterprise:

1. optimized multi-physics co-design of optical and terahertz properties (such as losses, power, linewidth, efficiency, power consumption, and dissipation) of miniaturized chips,
2. in-line control of the dispersion, spectrum, and temporal properties of the optical and telecom laser light necessary for the operation of the hybrid terahertz-optical chips and,
3. system-level design, including complex chip-scale architectures, ideally on large-scale wafers with efficient coupling in-and-out as well as out-of-chip pre- and post-conditioning of both terahertz and optical counterparts.

II. PICs FOR TERAHERTZ GENERATION

Current approaches for the generation of terahertz waves inside photonic integrated circuits rely mainly on the following three distinct principles, summarized in Fig. 2:

1. $\chi^{(2)}$-driven non-linear down-conversion (optical rectification) inside PICs: an optical pulse containing a broadband spectrum is rectified as it propagates along a transparent nonlinear waveguide. A terahertz antenna patterned around the waveguide efficiently emits the terahertz wave that is generated in the portion of the waveguide enclosed by the antenna and that matches in frequency the resonance and the bandwidth of the antenna. The antenna design determines the direction in which the terahertz is emitted. The maximal emission bandwidth is limited by the chirp of the pump pulse, phase matching, and absorption.

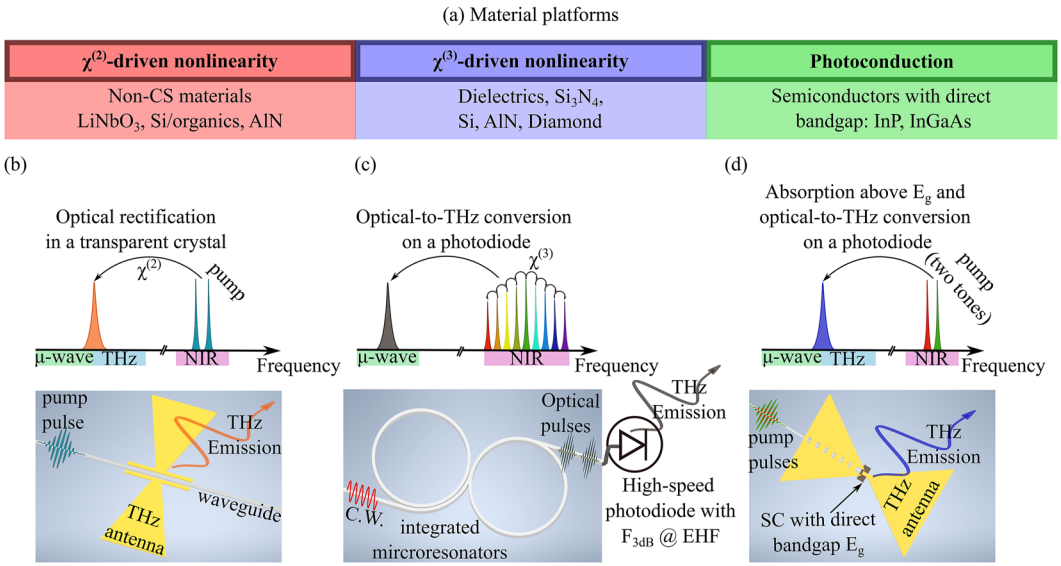

FIG. 2. PICs for terahertz generation. (a) Commonly used material platforms for terahertz generation in photonics integrated circuits: non-centrosymmetric (CS) materials such as lithium niobate ($LiNbO_3$), hybrid Silicon (Si)/organics, and aluminum nitride (AlN) exhibit second-order nonlinearity, making them suitable for $\chi^{(2)}$-driven nonlinear down conversion. Centro-symmetric materials with zero second-order nonlinearity such as silicon nitride (Si_3N_4) are commonly used for the $\chi^{(3)}$-driven generation of Kerr combs. Other dielectrics, such as silicon, diamond, and non-centrosymmetric materials with a large third-order nonlinear coefficient such as aluminum nitride and lithium niobate can also be used for Kerr comb generation. Semiconductors (SC) with a direct bandgap such as indium gallium arsenide (InGaAs) and indium phosphide (InP) are favorable for P-doped/intrinsic/N-doped (PIN) semiconductor photodiodes for photoconduction. Three distinct principles for terahertz generation in PICs: (b) $\chi^{(2)}$-driven non-linear down-conversion (optical rectification): a near-infrared (NIR) light pulse (green, which can be from a frequency comb or from the beating of two optical frequencies) is rectified by propagating through a nonlinear waveguide. The THz antenna efficiently emits the THz wave (orange wave) that matches in frequency the resonance and the bandwidth of the antenna. (c) $\chi^{(3)}$-driven nonlinearity: Optical Kerr combs (black pulses) are generated within a microresonator driven by a near-infrared continuous wave (C.W.) (red wave). A high-speed photodiode with a 3 dB bandwidth at extremely high frequencies (EHFs), for example, a uni-traveling carrier photodiode, is required for optical-terahertz conversion off-chip and emission of the terahertz wave (gray wave). (d) Waveguide-integrated photoconduction: By superpositioning two continuous waves with a frequency difference at microwave (μ-wave)/THz frequency, an optical beat note is generated (a green pulse) and fed into a PIN photodetector where the intrinsic region has a direct bandgap E_g. Through light absorption, a transient photocurrent at the beating frequency is generated, which drives the antenna to re-emit the broadband THz pulse (blue wave).

The bulk polarization induced by optical rectification can be derived as[41]

$$P_0^{(2)}(\Omega) = \frac{1}{2}\varepsilon_0\chi^{(2)}(\Omega,\omega_0)(E_0 * E_0^*)(\Omega), \quad (1)$$

where $\chi^{(2)}(\Omega,\omega_0)$ is the effective second order nonlinear susceptibility relevant for optical rectification at a pump frequency ω_0 and does not change significantly in the frequency range $(\omega_0-\Omega,\omega_0+\Omega)$. Using the Fourier transform of laser intensity, $I_{op}(\Omega) = \frac{\varepsilon_0 n(\omega_0)c}{2}(E_0 * E_0^*)(\Omega)$, this polarization (along the z-axis) can be rewritten as

$$P_0^{(2)}(\Omega) = \frac{\chi^{(2)}(\Omega,\omega_0)}{n(\omega_0)c} I_{op}(\Omega), \quad (2)$$

where $n(\omega_0)$ and c are the refractive index of the interaction medium at the pump frequency and speed of light, respectively. The generated terahertz field (generated by solving non-linear Maxwell's equation in the frequency domain) is

$$|E_{\mathrm{THz}}(\Omega)| = \frac{\mu_0\chi^{(2)}(\Omega,\omega_0)}{n(\omega_0)(n(\Omega)+n_g)} I_{op}(\Omega)\Omega l_{eff}(\Omega), \quad (3)$$

where $l_{eff}(\Omega) = \frac{\exp\left(-i\frac{\Omega n(\Omega)}{c}L\right)-\exp\left(-i\frac{\Omega n_g}{c}L\right)}{i\frac{\Omega}{c}(n(\Omega)-n_g)}$ is the effective generation length, and L is the geometric interaction length. The L-dependence of the generated electric field comes directly from $l_{eff}(\Omega)$, and it is strongly dependent on the material dispersion because of $n(\Omega)-n_g$; $n(\Omega)$ and n_g are the refractive index at the terahertz frequency and the group refractive index at the pump frequency, respectively. Clearly, employing materials with a large second-order susceptibility and a large interaction length between the optical and terahertz fields (assuming $l_{eff} \sim L$) can maximize the generated terahertz field through $\chi^{(2)}$-driven nonlinearity.

2. $\chi^{(3)}$-driven generation of optical Kerr combs in PICs, followed by subsequent optical-terahertz conversion at a photodiode (e.g., a uni-traveling carrier photodiode): a continuous-wave beam is sent through a high-Q on-chip resonator where a frequency comb is generated through four-wave mixing. The obtained broadband spectrum is then sent to a photodiode that is typically connected downstream from the photonic chip. The photodiode then performs the optical-to-terahertz transduction through its photocurrent. This approach is limited by the RC-time constant of the photodiode. The efficiency of the generated terahertz power depends on the carrier properties and the response time of the photodiode. The generated photocurrent from the optical excitation driven by mixing two continuous waves (with optical intensities I_{op1} and I_{op2}) with a frequency difference of $\Omega = \omega_1 - \omega_2$ at a photoconductive material (photomixing) can be expressed as[42]

$$I_{PC}(t) = \tau_c\mu_e E_{bias}\left(I_{op1} + I_{op2} + \frac{2\sqrt{I_{op1}I_{op2}}}{\sqrt{1+\Omega^2\tau_c^2}}\cos(\Omega t+\phi)\right), \quad (4)$$

where $\phi = \tan^{-1}(\Omega\tau_c)$. τ_c, μ_e, and E_{bias} are carrier lifetime, carrier mobility, and the bias field, respectively. The radiated terahertz field from this oscillating photocurrent is proportional to its derivative ($E_{\mathrm{THz}} \propto \frac{dI_{PC}}{dt}$), and the radiated terahertz power at frequency Ω is

$$P_{\mathrm{THz}}(\Omega) = 2R_A E_{bias}^2 I_{op1} I_{op2}\frac{\tau_c^2\mu_e^2}{1+\Omega^2\tau_c^2}, \quad (5)$$

where R_A is the radiation resistance. For a Hertzian dipole, R_A is equal to $80\pi^2\left(\frac{d}{\lambda}\right)^2$, where d is the length of the dipole and λ is the free space wavelength. Therefore, high-power terahertz radiation via photomixing requires high optical intensities, a large bias field, and a high-mobility material.

3. Photoconduction directly on-chip inside semiconducting PICs: optical pulses from an external fiber-based source are guided on-chip toward a heterogeneously integrated semiconducting patch that is surrounded by a terahertz antenna. At this patch, which is purposefully designed to contain many defects, generated photocarriers build up an ultrafast current. The defects then decelerate the carriers, which leads to a terahertz waveform that is generated locally and efficiently emitted by the antenna. The maximal bandwidth is determined by the properties of the defects.

The time-dependent photocurrent in this case is the convolution of the optical pulse envelope and the impulse response of the photoconductive material. Considering the optical pulse is a Gaussian with a pulse duration of $2\sqrt{\ln 2}\tau_p$, the photocurrent can be expressed as[42]

$$I_{PC}(t) = \frac{\sqrt{\pi}}{2}\mu_e E_{bias} I_{op}^0\left[exp\left(\frac{\tau_p^2}{4\tau_c^2}-\frac{t}{\tau_c}\right)\cdot erfc\left(\frac{\tau_p}{2\tau_c}-\frac{t}{\tau_p}\right) - exp\left(\frac{\tau_p^2}{4\tau_{cs}^2}-\frac{t}{\tau_{cs}}\right)\cdot erfc\left(\frac{\tau_p}{2\tau_{cs}}-\frac{t}{\tau_p}\right)\right], \quad (6)$$

where τ_s, τ_c, μ_e, E_{bias}, and I_{op}^0 are momentum relaxation time, carrier lifetime, carrier mobility, bias field, and optical intensity, respectively. Erfc is the complementary error function $\mathrm{erfc}(x) = 1-\mathrm{erf}(x) = \frac{2}{\sqrt{\pi}}\int_x^\infty \exp(-t^2)dt$ and $\tau_{cs}^{-1} = \tau_c^{-1} + \tau_s^{-1}$. Similar to the previous part, the radiated terahertz field from the photocurrent is proportional to its derivative ($E_{\mathrm{THz}} \propto \frac{dI_{PC}}{dt}$).

It should be pointed out that the photoconductive antennas can also operate under continuous wave pumping and have shown emitters up to a 3.5 THz bandwidth.[46,47]

Two fundamental properties make the above-mentioned approaches viable for seamless terahertz generation alongside photonics. On the one hand, the mismatch between the wavelength of terahertz radiation (a few tens to thousands of micrometers) and the one of optical radiation (around 1 μm) is a coincidental match that allows the patterning of efficient terahertz cavities (antennas or LC resonators) in the immediate vicinity of photonic structures quasi-independently. In this spirit, for example, on-chip, rib, or slot waveguides can be routed into the gap formed by two electrodes of a metallic antenna, where the generation and extraction of a terahertz

TABLE I. State-of-the-art of the integrated devices for terahertz generation. CW = continuous wave, UTC-PD = unitravelling carrier photodiode, InGaAs = indium gallium arsenide, InP = indium phosphide, InAs = indium arsenide, P-I-N = positive-intrinsic-negative, PD = photodiode, DR = dynamic range, IF = intermediate frequency, BW = bandwidth, P_{THz} = terahertz power, P_{op} = optical average power, V_{bias} = bias voltage, V_{pp} = peak–peak voltage, U_{pump} = pump energy, U_{THz} = terahertz energy, Ω = terahertz frequency, I_{PC} = photoconductive current.

References	Schematic of the devices	Mechanism	Integration level	Description and properties
48 and 62	Germanium on Silicon 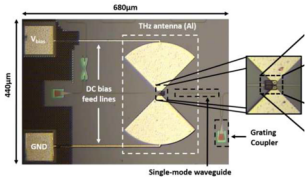	A photoconductive terahertz antenna is excited by an optical laser pulse at 1550 nm, coupled through an integrated waveguide	On-chip: A waveguide coupled photoconductive switch + terahertz antenna Off-chip: Pulsed laser	Terahertz pulse width = 1.14 ps, V_{bias} = 3.5 V, BW = 1.5 THz, $\overline{P_{THz}}$ = 337 μW at Ω = 176 GHz, conversion efficiency = 3.6×10^{-5}, die area: 440 × 680 μm^2
49	InP/InGaAs UTC-PD 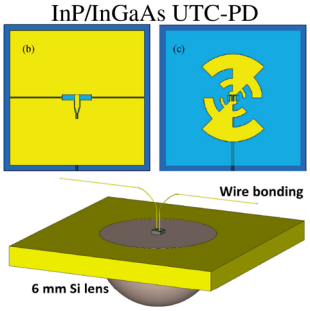	An optical beat, at the difference frequency between two CW lasers at around 1550 nm, is fed into the UTC-PD through a coupled waveguide and generates a photocurrent. An antenna is attached to the UTC-PD to radiate this photocurrent into free-space	On-chip: A waveguide coupled UTC-PD + terahertz antenna Off-chip: CW lasers	P_{THz} = 3.8 dBm at Ω = 100 GHz, Ω up to 500 GHz; DR = 105 dB at 130 GHz; responsivity = 0.105 A/W after packaging (0.25 A/W before packaging); photodiode area: 30 μm^2
54	Thin-film Lithium niobate 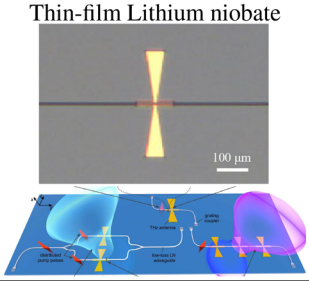	A terahertz antenna emits a terahertz signal generated through optical rectification of a femtosecond pulse at 1550 nm guided along a nonlinear waveguide	On-chip: Lithium niobate waveguide (nonlinear media) + terahertz antenna Off-chip: Pulsed laser	E_{THz} = 1 V/m, U_{THz} ~ 10^{-20} J with U_{pump} = 100 pJ, conversion efficiency = 10^{-10}, Ω = between 180 and 680 GHz. Series and parallel antenna geometry for engineering the terahertz pulse shape
61	P-I-N photodiode on InP 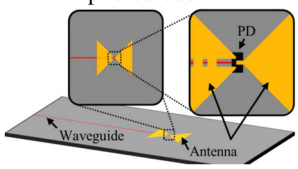	An optical beat, at the difference frequency between two CW lasers at around 1550 nm, is fed into the PD emitter through a coupled waveguide and generates a photocurrent. An antenna is attached to the PD to radiate this photocurrent into free-space	On-chip: A waveguide coupled PD + terahertz antenna Off-chip: Pulsed laser	I_{PC} = 10 mA, P_{op} = 15 dBm, P_{THz} = −15 dBm at Ω = 300 GHz, responsivity = 0.32 A/W, chip area = 1.5 × 3 mm^2

TABLE I. (*Continued*.)

References	Schematic of the devices	Mechanism	Integration level	Description and properties
43	Fused silica microtoroid 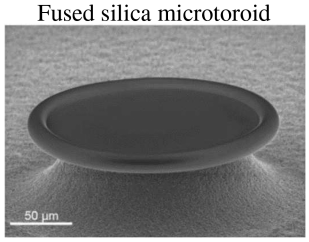	A CW laser at 1550 nm pumps a microresonator and generates a soliton microcomb. The output of the resonator is amplified and transduced to terahertz by a UTC-PD	On-chip: Microresonator Off-chip: CW laser + UTC-PD	I_{PC} = 7 mA, P_{THz} = −10 dBm (Ω = 331 GHz). P_{IF} = −50 dBm and amplified using low-noise RF amplifiers. Low phase noise above 1 MHz offset frequencies
44	Silicon Nitride 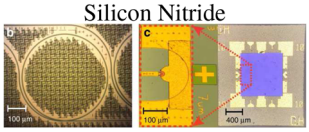	A CW laser at 1550 nm pumps a microresonator to generate a soliton microcomb. The output of the resonator is amplified and then transduced to terahertz by a modified UTC-PD	On-chip: Microresonator on chip 1, integrated modified UTC-PD on chip 2 Off-chip: CW laser	P_{THz} = 7 dBm at I_{PC} = 22.5 mA, Ω = 100 GHz. V_{bias} = −3.6 V. Device width = 8 μm
45	Silicon Nitride 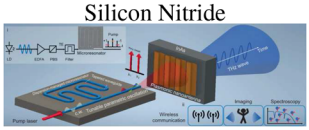	A CW laser (1520–1610) nm pumps a microresonator and generates a signal/idler. The resonator output is detected by a plasmonic photoconductive nanoantenna array photomixer	On-chip: Microresonator Off-chip: Laser diode + InAs plasmonic nanoantenna	Ω = 0.33–2.3 THz, frequency tuning = 20 GHz, P_{THz} = 10 μW(−20 dBm) at Ω = 651 GHz, the IF signal is amplified by an electrical amplifier to −10 dBm

wave actually happen. This allows a two-step optimization in which the optical fields remain tightly confined to the core of the waveguides, thus fully exploiting the nonlinearity within, while the properties of the extracted terahertz fields (e.g., the farfield pattern, the center frequency, the linewidth) are directly dependent on the antenna dimensions as well as on the spectral and phase characteristics of the optical light. On the other hand, the photonic circuit can be assembled from individual components that are linked via passive waveguides. In this way, the optical rectification, photoconduction, or terahertz generation may be localized far from other components that may, for example, fulfill the purpose of preconditioning the optical beams, e.g., by generating chip-scale Kerr combs.

We present an overview of state-of-the-art devices for terahertz generation in integrated photonic circuits in Table I. Photoconduction has been demonstrated in silicon waveguides using Germanium photoconductive antennas,[48] in indium phosphide waveguides using indium phosphide/indium gallium arsenide uni-traveling carrier photodiodes,[49–51] and in other platforms (not shown in the table) such as aluminum gallium arsenide waveguides using low-temperature grown gallium arsenide photoconductive antennas.[52] Optical rectification, on the other hand, has been a valuable alternative to reaching high terahertz frequencies. Early attempts demonstrated terahertz emission up to 6 THz[53] from a metal-infused waveguide in bulk lithium niobate. More recently, the low optical loss of the thin film lithium niobate platform[54] provided access to both the nanoscale design of waveguides and printed antennas and the macroscale design of the entire circuit. These offered unprecedented control over the synthesis of terahertz waveforms up to 680 GHz (3-dB cutoff of 400 GHz), including their phase, amplitude, polarization, and farfield of the emitted radiation. In the case of $\chi^{(3)}$ generation techniques, micro-resonator frequency combs in silicon nitride have been successfully employed in combination with out-of-chip uni-traveling carrier photodiodes to generate ultra-low noise RF carriers in the X and K bands,[18] but also at 331[43] or 560 GHz.[55] Kerr combs have also been used with out-of-chip photoconductive antennas to generate terahertz waves up to 2.3 THz.[45] To date, to the best of our

knowledge, a demonstration of heterogeneous integration of the uni-traveling carrier photodiode or the photoconductive antenna directly with a Kerr comb is missing. This may only be a matter of time since there have been several demonstrations of uni-traveling carrier photodiodes or other high-frequency photodiodes being integrated with photonic circuits, for example, indium gallium arsenide/indium phosphide-based uni-traveling carrier photodiodes with lithium niobate waveguides using SU-8 as a bonding layer (3-dB bandwidth of 80 GHz),[56] Germanium diodes integrated with Silicon waveguides (3-dB bandwidth of 265 GHz),[57] or Graphene photodiodes with plasmonic waveguides (3-dB bandwidth of 110 GHz).[58] In addition, it seems that efficient emission is rather limited to the sub-terahertz regime since both the P-doped/intrinsic/N-doped semiconductor photodiode and the uni-traveling carrier photodiode feature a strong decay of 20 dB per decade in the power of emitted terahertz at frequencies above about 300 GHz,[50,59,60] due to their intrinsic RC time constant. Nevertheless, they have been employed as transceivers in an optical communication link at 300 GHz.[61]

III. PICs FOR TERAHERTZ DETECTION

Current approaches for the detection of terahertz waves inside integrated photonic circuits rely mainly on the following two distinct principles, summarized in Fig. 3:

1. $\chi^{(2)}$-driven electro-optic sampling in miniaturized interferometers: a terahertz wave is shone onto a chip-scale antenna, which collects and confines it to the antenna gap. Optical nonlinear waveguides pass through this gap. Here, the terahertz wave introduces a refractive index change in the waveguide material that is proportional to the in-gap terahertz electric field. A femtosecond pulse traverses the antenna gap and experiences a phase delay that is directly proportional to the introduced refractive index change. By geometry, the duration when the two waves meet is a fraction of a terahertz period, thereby limiting the detection to a sub-terahertz cycle time window. The phase delay is transformed into an intensity modulation, which can conveniently be measured by a photodiode downstream from the photonic chip. In the case of integrated electro-optic terahertz detection with a Mach–Zehnder configuration, the intensity modulation is expressed as[63]

$$\Delta I(t) = \frac{I_p r_{33} n_{opt}^2 l_{\mathrm{int}} \Omega E_{\mathrm{THz}}(t) \Gamma_c n_g FE}{c}, \tag{7}$$

where I_p, r_{33}, n_{opt}, l_{int}, Γ_c, and FE are probe intensity, electro-optic coefficient, the refractive index at the probe frequency, interaction length, mode overlap between the terahertz and optical beam, and field enhancement, respectively. Sensitive terahertz detection with a high modulation efficiency, $\eta = \frac{\Delta I}{I_p}$, requires waveguide materials with a high electro-optic coefficient and large refractive index at optical frequencies, a high group refractive index, and antennas with a large interaction length, a high mode overlap with the optical field propagating through the waveguides, and a large field enhancement.

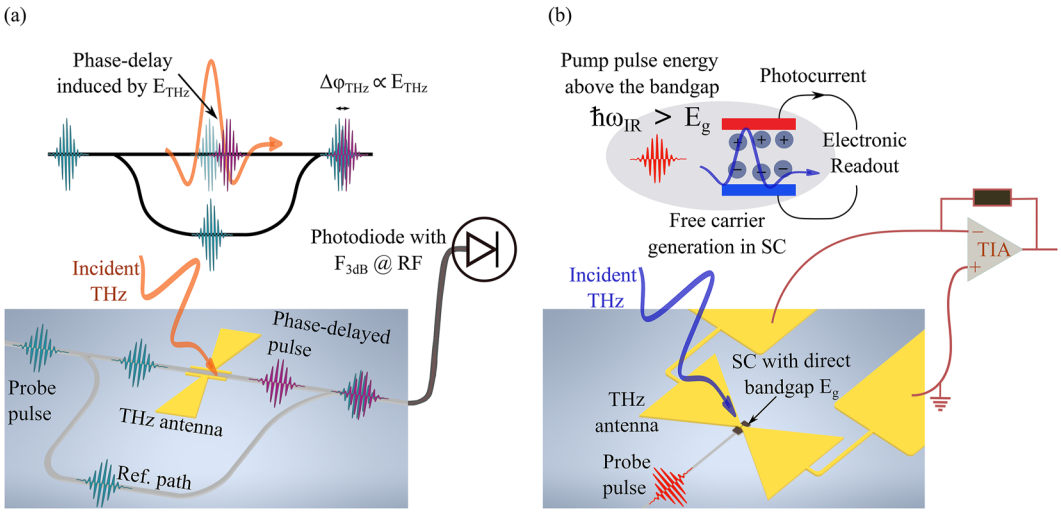

FIG. 3. PICs for terahertz detection. Two distinct principles for terahertz detection in photonics integrated circuits: (a) $\chi^{(2)}$-driven electro-optic sampling in a miniaturized interferometer: A femtosecond pulse (green pulse) passes through a Mach–Zehnder interferometer waveguide structure. The pulse transverse to the THz antenna gap experiences a phase delay ($\Delta\phi_{\mathrm{THz}}$) proportional to the incident THz electric field (orange wave). The interference between the phase-delayed pulse (violet pulse) and the pulse passing through the reference (Ref.) path is transformed into an intensity modulation and can be measured by a photodiode with a 3 dB bandwidth at radio frequencies (RF), a few KHz to a few tens of MHz downstream from the photonic chip. (b) Photoconduction: Similar to terahertz generation via photoconduction, the absorption of an optical beat note (red pulse) in a semiconducting (SC) PIN structure, where the intrinsic region has a direct bandgap E_g, generates a transient photocurrent. The collected incident THz wave (blue wave) by the THz antenna acts as a drive voltage and accelerates the generated carriers toward the contacts, where a current can be read out. The photocurrent is measured electronically after amplification with a trans-impedance amplifier (TIA).

TABLE II. State-of-the-art of the integrated devices for terahertz detection. InGaAs = indium gallium arsenide, InP = indium phosphide, RF = radio frequency, CW = continuous wave, DR = dynamic range, PCA = photoconductive antenna, E_{THz} = terahertz field, BW = bandwidth, Ω = terahertz frequency of wavelength λ_{THz}, P_p = probe power, η = modulation efficiency, I_{PCD} = photoconductor current, I_{dark} = dark current, V_{bias} = bias voltage, SPP = surface plasmon polariton.

References	Schematic of the devices	Mechanism	Integration level	Description and properties
65	Hybrid silicon-organic 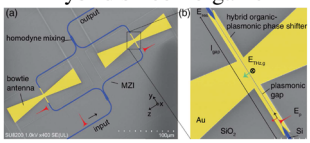	The terahertz wave introduces a refractive index change (Δn) in the nonlinear organic material, proportional to the in-gap E_{THz}. A femtosecond pulse at 1550 nm traverses the antenna gap and experiences a phase delay directly proportional to the introduced Δn	On-chip: Mach–Zehnder interferometer + terahertz antenna Off-chip: Pulsed laser + slow photodiode (F_{3dB} at RF frequency range)	Sensitivity: $E_{THz} < 20$ V/m, $\eta = 0.7\%$ for Ω = 220 GHz, DR > 70 dB in intensity at 500 ms integration. Single-photon cooperativity = 1.6×10^{-8}. Field confinement ~$10^{-9}(\lambda_{THz}/2)^3$, $P_p = 1$ μW
63	Hybrid silicon-organic 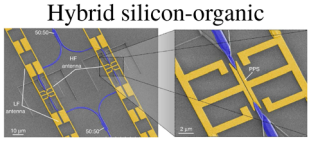	Same as above	On-chip: Mach–Zehnder interferometer + terahertz antenna Off-chip: Pulsed laser + slow photodiode (f_{3dB} at RF frequency range)	$\frac{\eta}{E_{THz}} = 7.62 \times 10^{-6}$ (mV^{-1}). Ω = 1.2, 2.4 THz. BW = 2.5 THz, DR = 65 dB. Field confinement = $10^{-8}(\lambda_{THz}/2)^3$, $P_p = 63$ nW
66	Iron-doped InGaAs on InP 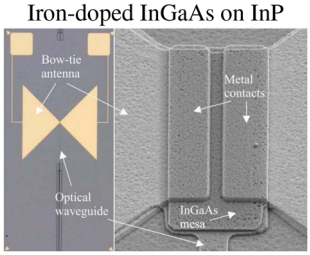	A photoconductive material is pumped by a CW laser above its bandgap, creating free carriers. A terahertz antenna collects and confines the terahertz wave to the gap. The wave acts as a drive voltage and accelerates the generated carriers toward the contacts, resulting in a photocurrent that is proportional to the in-gap E_{THz}	On-chip: A waveguide coupled photoconductive switch + terahertz antenna Off-chip: CW laser + RF trans-impedance amplifier	$P_p = 30$ mW. $I_{PCD} = 350$ μA, and $I_{dark} = 100$ μA. $V_{bias} = 0.5$ V. I_{PCD} is 6.8 times higher than the top-illuminated PCA. Below 2 THz, the detected E_{THz} is up to 7.3 times higher compared to the top-illuminated device

TABLE II. (*Continued.*)

References	Schematic of the devices	Mechanism	Integration level	Description and properties
58	Graphene on silicon 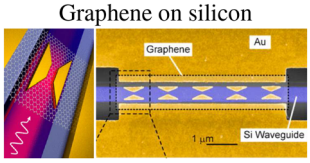	An optical beat note (beating at a THz frequency) traverses the silicon waveguide. Its field couples evanescently to graphene by exciting SPPs in the metallic structures. The absorbed light changes the conductivity and eventually the photocurrent in graphene under a bias voltage across the metallic pads	On-chip: A waveguide coupled to a graphene layer + terahertz antenna Off-chip: CW laser + RF power meter	Internal quantum efficiency (IQE) = 87%. Photoresponsivity: 0.5 A/W. V_{bias} = −0.4 V. P_p = 80 μW. BW = 110 GHz
57	Germanium on silicon 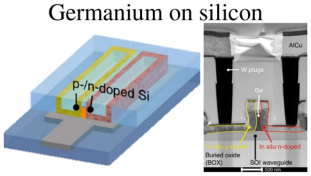	An optical beat note (beating at THz frequency) is fed into the waveguide and the PIN photodiode. Through light absorption, a transient photocurrent at the beating frequency is generated under a bias voltage	On-chip: A waveguide coupled to a germanium photodetector Off-chip: CW laser + RF power meter	I_{dark} = 100–200 nA. V_{bias} = −2 V. Responsivity: 0.32 A/W with BW = 265 GHz at I_{PCD} = 1 mA. Responsivity of 0.45 A/W with BW = 240 GHz at I_{PCD} = 1 mA

2. Photoconduction-based detection: a photoconductive material is pumped by a femtosecond laser pulse above its bandgap, creating free carriers. A terahertz antenna is patterned on top of the photoconductive material. It collects and confines the terahertz wave to the gap. The wave acts as a drive voltage and accelerates the generated carriers toward the contacts, where a current can be read out. By geometry, the read-out current is directly proportional to the amount of generated photocarriers and to the in-gap terahertz electric field at the moment when the probe pulse arrives. It can therefore be used to retrieve the terahertz transient on sub-cycle temporal scales. For a photoconductive detector, one can drive the terahertz electric field as[64]

$$I_{PCD}(\tau) = \frac{\mu_0 e P_G T_{12} \lambda}{hc\Sigma} \int_{-\infty}^{+\infty} E_{\mathrm{THz}}(t)\Phi(t-\tau)dt, \qquad (8)$$

where $\Phi(t), T_{12}, P_G, h$, and Σ are the temporal evolution of the conductivity response of the semiconductor, the Fresnel transmission coefficient for laser at wavelength λ, the average power entering the semiconductor substrate of the photoconductive switch, Planck's constant, and the standard deviation of the laser Gaussian spatial profile, respectively. Routing the probe pulse via waveguides to the antenna gap (which has dimensions of a few micrometers) is crucial to delivering maximal power to the photoconductive material, especially when such a spot size would be difficult to achieve using free-space focusing optics.

Two fundamental properties make the above-mentioned approaches viable for seamless terahertz detection by photonics. On the one hand, careful engineering of the cross-section of on-chip waveguides (and therefore their group velocity dispersion) allows femtosecond pulses to travel with very low temporal broadening along a few millimeters of total relevant waveguide lengths until the antenna gap where the detection happens. This aspect is crucial, as the temporal resolution of the field measurement is equal to the temporal width of the femtosecond pulse at the location of detection. On the other hand, terahertz antennas allow for the confinement of terahertz fields to highly subwavelength antenna gaps. This confinement increases the local amplitude of the terahertz wave by a factor of 100–1000 compared to free space. This introduces, in the case of $\chi^{(2)}$-based detection, a large refractive index change inside the nonlinear waveguide and, in the case of photoconduction, a large photocurrent.

We present an overview of state-of-the-art devices for terahertz detection in PICs in Table II. Co-integration of optical waveguides and terahertz antennas has been leveraged to achieve highly efficient detection of terahertz waves in a desired band (e.g., 300, 500, or 700 GHz),[65] with a maximal frequency demonstrated so far of

2.5 THz[63] using on-chip hybrid silicon-organic waveguides that exploit a strong $\chi^{(2)}$ nonlinearity in organic molecules in combination with strongly confining plasmonic slots and silicon-on-insulator waveguides. In parallel, waveguide-coupled photoconductive detectors using indium gallium arsenide phosphide/indium phosphide passive waveguides and iron-doped indium gallium arsenide photoconductive antennas were shown to have an improved responsivity of up to 2 THz compared to free-space illuminated photoconductive antennas, with a total detection bandwidth of up to 4 THz.[66] Moreover, several demonstrations of high-frequency photodiodes being integrated with photonic circuits such as germanium diodes integrated with silicon waveguides (3-dB bandwidth of 265 GHz)[57] or graphene photodiodes with plasmonic waveguides (3-dB bandwidth of 110 GHz)[58] are among the state-of-the-art devices for terahertz detection.

We note that various other miniaturized terahertz detection and generation schemes have been reported in the literature, and in this perspective, we focus only on those that have been shown to work in integrated photonic circuits.

IV. MINIATURIZING TERAHERTZ-OPTICAL CHIPS

Notwithstanding the currently undergoing research efforts summarized in Secs. II and III, we foresee that fundamental properties will play a major role in the successful deployment of terahertz photonics by integrated circuits.

A. Losses

Many of the benefits of integrated photonics are rooted in the possibility of propagating optical pulses with extremely low loss along waveguides that can be several millimeters to centimeters in length. This is essential, both in schemes that employ several parallel waveguides (e.g., as is the case of on-chip interferometers), one single long waveguide (e.g., when several antennas are pumped subsequently), or where high-Q resonators are an absolute requirement (e.g., in the generation of Kerr combs). In this respect, silicon-on-insulator, lithium niobate, and silicon nitride have excellent properties. For example, while organics suffer from high losses of 250 dB/mm in plasmonic waveguides, these can be significantly reduced to 0.2–2 dB/mm in slot waveguides.[67,68] Lithium niobate rib waveguides feature losses below 0.7 dB/cm. This is the case even when antennas with a gap width of 3 μm were patterned around the waveguides. Losses below 0.01 dB/cm can be achieved for gaps larger than 6–7 μm.[54] Silicon nitride, on the other hand, reaches record quality factors.[69] Indium phosphide has a large optical gain and is mainly used in PIC telecommunication as a semiconductor optical amplifier; however, indium phosphide-based waveguides compared to silicon nitride have a much higher propagation loss (2–0.4 dB/cm) and bend radius (0.1 mm).[70]

In the same spirit, terahertz losses on-chip can hamper the widespread use of terahertz photonics. Coincidentally, both hybrid silicon-organic and lithium niobate use high-resistivity silicon as a substrate that has excellent transparency in the terahertz.[71] However, lithium niobate is known to have strong phonon resonances in the terahertz.[72,73] Here, the highly sub-terahertz-wavelength thickness of thin film lithium niobate comes in handy since the generation and detection of the terahertz waves happen just below the surface of the chip. This minimizes any propagation through the lossy material. Still, several fundamental questions need to be addressed. For example, if and to what extent the phonons present in these thin films limit the maximal bandwidth of detection and generation on-chip. In strong contrast to lithium niobate, organic materials have already been demonstrated in a neat form to generate extremely broadband terahertz radiation featuring no spectral gaps[74] otherwise present, e.g., in semiconductors that have strong phonon resonances in the terahertz. However, organic systems can also inherit a strong terahertz absorption if embedded into a polymer matrix, e.g., for purposes of achieving thick layers [organic molecules mixed with polymethylmethacrylate (PMMA) can have losses of about 60 dB/cm at 1 THz[75]]. In this context, exploration of other polymers that are low-loss in the terahertz (such as benzocyclobutene) may be envisioned. This is, however, not straightforward, as the interaction between the molecule and the polymer matrix plays a role in the achieved electro-optic coefficients and long-term stability at high temperatures.[76] In scenarios where thin layers of only a few hundred nanometers are sufficient, neat chromophore films are typically recommended to minimize terahertz absorption (see Refs. 63 and 65).

Besides the waveguides, the material losses in terahertz antennas and electrodes restrict the performance of the photonic devices. Ohmic losses increase in metals at high frequencies due to the skin effect. The skin depth of a conductor is the distance below its surface where the current density reaches 1/e of its value at the surface. The skin depth is inversely proportional to the square root of frequency and falls below 100 nm at 1 THz in gold, silver, copper, and aluminum.[77,78] Hence, their conductivity significantly drops at a thickness comparable to/smaller than the skin's depth. For instance, the conductivity of an 85 nm gold film drops to 33% (12%) of its bulk conductivity at room temperature (at 77 K).[79] Employing alternative conductive materials[80,81] such as dielectrics,[82,83] transparent conducting oxides,[84] and graphene[85] or nano/micro-structuring the pads to steer and control the current[28,86] are ideas worth considering to circumvent the total losses of a photonic terahertz-optical chip.

B. Dispersion

With the possibility to propagate optical and terahertz waves with minimal loss on-chip, perhaps the biggest advantage of integrated waveguides over bulk media is that they allow for engineering the dispersion. For instance, tailoring their geometrical parameters, such as width, height, etching depth, etc., can alter the effective index to take values between the one of the core and cladding (e.g., at 1550 nm, between ~2.3 and 1.5 in lithium niobate–silica waveguides, ~1.87 and 1.5 in organic–silica waveguides, and ~2 and 1.5 in silicon nitride–silica waveguides). Interested readers can find here the refractive index of lithium niobate,[87] the organic molecule JRD1 in PMMA,[88] the organic salts 4-*N*,*N*-dimethylamino-4′-*N*′-methyl-stilbazolium tosylate (DAST)[89,90] and 4-*N*,*N*-dimethylamino-4′-*N*′-methyl-stilbazolium 2,4,6-trimethylbenzenesulfonate (DSTMS),[91,92] or silicon nitride.[93] The effective index is directly linked to phase matching, and its control allows the suppression of unwanted nonlinear processes and the optimization of terahertz generation and detection. In addition, the group velocity dispersion can be changed,

e.g., in lithium niobate, up to a few hundred of $\frac{ps^2}{mm}$, two orders of magnitude larger than the intrinsic material dispersion in the bulk.[94] This can be exploited to introduce chirp or compress pulses. The maximal bandwidth of detection and generation of terahertz waves can thereby be optimized since it is strictly related to the pulse width over the entire length of the interaction. Furthermore, dispersion control has been largely exploited in various on-chip platforms for Kerr combs, supercontinuum generation,[95,96] solitons formation,[97,98] femtosecond pulse generation,[99] etc.

In the context of the dispersion of the terahertz wave, the detailed antenna geometry influences its group delay.[54]

C. Nonlinearities

In general, materials with high nonlinear coefficients are recommended as they maximize conversion efficiency. However, for the terahertz, exploration of the materials with the largest nonlinearities was only partially possible. In Table III, we report the nonlinear coefficients of platforms for integrated photonics. At the top of the table, we report—for comparison—the most prominent materials for terahertz, zinc telluride and gallium phosphide. Visibly, they have quite low nonlinearities. Their advantage is that they allow high optical powers and have favorable phase-matching properties when used with femtosecond lasers at 780 or 1064 nm—two equally important considerations when maximizing the efficiency of a nonlinear process. Materials with higher nonlinearities like lithium niobate feature extreme phase mismatch (the terahertz refractive index is much larger than the optical one due to the strong phonon resonances). In this respect, integrated circuits overcome the limitations of bulk crystals: waveguide engineering can improve phase matching, and chip-scale resonators recirculate the input optical power as a means to increase the total conversion efficiency.

The most prevalent materials for second-order optical processes for terahertz generation and detection in PICs are hybrid silicon-organic[63,65] and lithium niobate.[54] As shown in the table, organic molecules have among the highest nonlinearities. These demonstrations have leveraged either the d_{33} or the r_{33}, the strongest ones in both hybrid silicon-organic and lithium niobate. However, exploration of other components of the electro-optic tensor is possible since crystals with other cuts are available (x- and z-cut). Alternatively, electric field poling[114,115] can be employed to orient the crystal in a desired direction. In addition, they have been shown to work at cryogenic temperatures.[68,116]

TABLE III. Nonlinear optical properties of material platforms commonly used in integrated photonics and free space terahertz optics. ZnTe = zinc telluride, GaP = gallium phosphide, GaAs = gallium arsenide, $LiNbO_3$ = lithium niobate, DAST = 4-*N*,*N*-dimethylamino-4′-*N*′-methyl-stilbazolium tosylate, DSTMS = 4-*N*,*N*-dimethylamino-4′-*N*′-methyl-stilbazolium 2,4,6-trimethylbenzenesulfonat, Si = silicon, SiO_2 = silicon oxide, Si_3N_4 = silicon nitride, AlN = aluminum nitride. * All the refractive indices are given at wavelength λ = 1550 nm, and o/e are ordinary/extraordinary axis.

Material	Refractive index (n_0)*	Second-order nonlinear coeff. (pm/V)	Electro-optic coefficient (pm/V)	Nonlinear refractive index (n_2) (nm^2/W)	References
ZnTe(110)	2.73	d_{41} = 52 (at 1320 nm)	r_{41} = 4 (at 1060 nm)	7.1 (at 790 nm)	100–103
GaP(110)	3.05	d_{41} = 0.42 d_{36} = 70.6 (at 1060 nm)	r_{41} = 0.87 (at 1060 nm)	6.99 (at 1040 nm)	104–107
GaAs	3.38	d_{36} = 170 119 (at 1064, 1533 nm)	r_{41} = 1.43 (at 1550 nm)	26 (at 1550 nm)	106 and 94
$LiNbO_3$	2.21 (o) 2.14 (e)	d_{31} = −4.3 d_{22} = 2.10 d_{33} = −27.0 (at 1064 nm)	r_{13} = 9.6 r_{22} = 6.8 r_{33} = 30.9 r_{51} = 32.6 (at 633 nm)	0.18 (at 1550 nm)	94 and 108
JRD1 (organic)	1.84	⋯	r_{33} = 370 (at 1550 nm)	⋯	109
DAST (organic)	2.1	d_{11} = 1010, 290 (at 1318, 1542 nm)	r_{11} = 92, 47 (at 720, 1535 nm)	1.65 (at 1550 nm)	110 and 111
DSTMS (organic)	2.05	d_{11} = 214 (at 1900 nm)	r_{11} = 32 (at 1900 nm)	1.65 (at 1550 nm)	91 and 92
Si	3.48	0	0	5 (at 1550 nm)	94
SiO_2	1.44	0	0	0.03 (at 1550 nm)	94 and 112
Si_3N_4	2	0	0	0.25 (at 1550 nm)	94 and 112
AlN	2.12 (o) 2.16 (e)	d_{31} = 1.6 d_{33} = 4.7 (at 1550 nm)	r_{13} = 0.67 r_{33} = −0.59 (at 633 nm)	0.23 (at 1550 nm)	94, 112, and 113

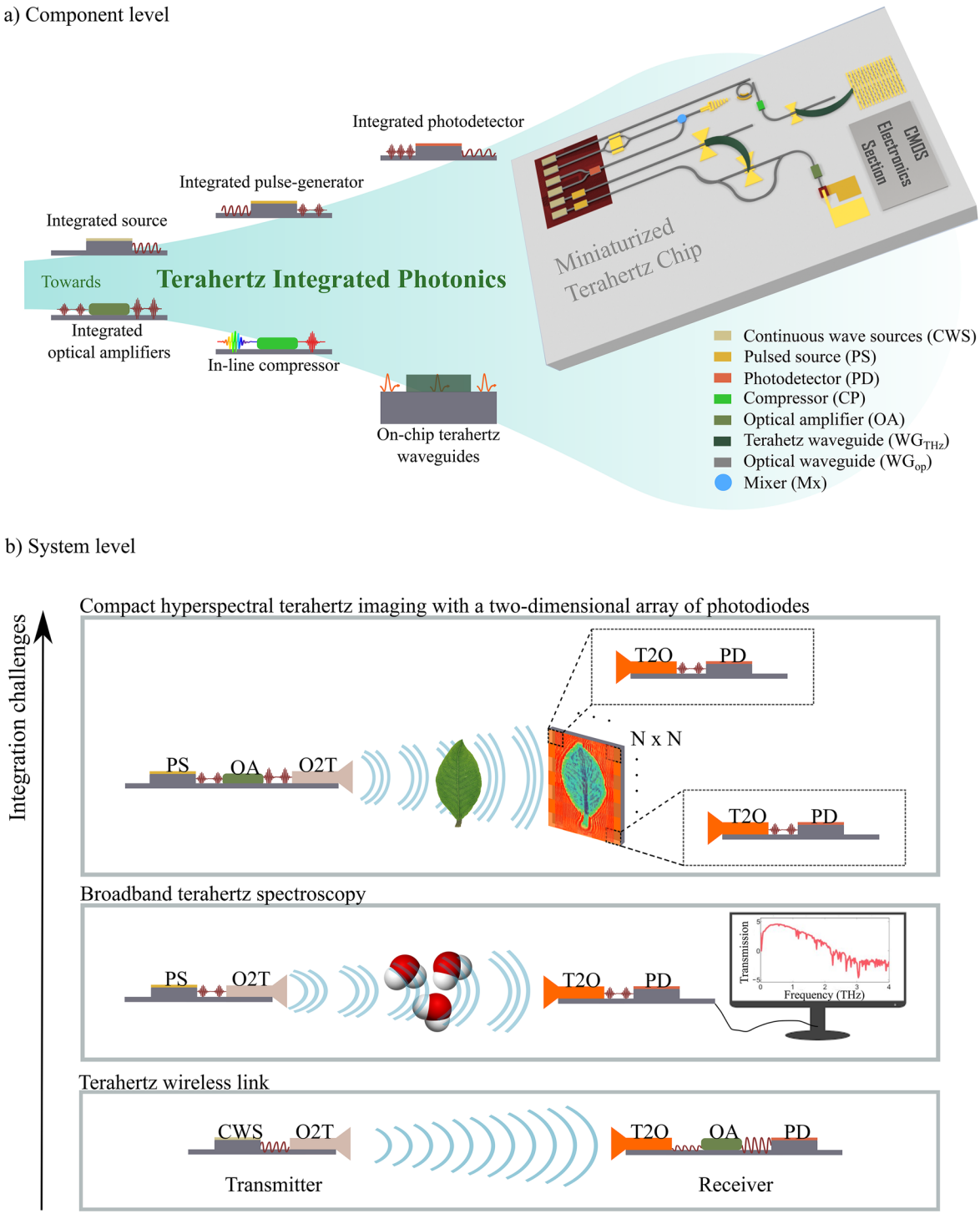

FIG. 4. Milestones ahead toward terahertz integrated photonics. (a) Component-level perspective: To accomplish a fully on-chip photonic-based system operating at terahertz frequencies, several fundamental components such as continuous wave and pulsed sources, photodetectors, optical amplifiers, terahertz waveguides, and in-line compressors remain to be developed. Hybrid/heterogeneous integration, in a low-cost and mass-manufacturable way, is a crucial criterion to fulfill the physical requirements for high-performance PICs. (b) System-level perspective: several components of panel (a) may be assembled into a system with applications in terahertz wireless links, broadband spectroscopy, and phase-resolved hyperspectral terahertz imaging. All components may benefit the applications depicted in Fig. 1. O2T and T2O are optical-to-terahertz and terahertz-to-optical converters, respectively.

In the context of Kerr combs, silicon nitride and aluminum nitride are among the most mature material platforms. Interestingly, however, silicon nitride also does not have the highest nonlinearity. The lower optical loss of chip-scale ring resonators compared to other platforms nevertheless positioned them in the leading position because of the overall superior efficiency of four-wave mixing. For example, finesses above 600 were demonstrated in this material.[69]

From a more fundamental point of view, we foresee that the biggest challenge to tackle is the generation of high-power terahertz radiation. This is irrespective of the material or principle used. The small cross-section of waveguides imposes a limit on the in-device intensity before other nonlinear effects start to dominate. This, in turn, limits the total pulse energy and, thereby, the maximal number of terahertz sources that can be generated. Workarounds need to foster a more efficient depletion of the pump, e.g., by using long or parallel waveguides or high-Q resonators.

V. SCIENCE AND APPLICATIONS AHEAD

The hybrid terahertz-optical platforms discussed earlier allow—for the first time—compact devices that transduce terahertz waves back and forth to telecom waves, departing from titanium sapphire laser wavelengths. This is promising because fiber technologies are rich and performant in this range. However, their wide adoption critically requires further integration efforts both at the component level and at the system level. The most pressing questions we foresee toward this goal are: 1. how to efficiently generate, distribute, guide, and collect terahertz waves inside miniaturized chips; 2. how to make terahertz systems more streamlined, e.g., using low-loss fiber-to-chip, laser-to-chip, and chip-to-photodiode interfaces for a seamless in-line integration of the photonic chip with, e.g., upstream semiconductor laser diodes, miniaturized pulsed lasers, as well as downstream high-frequency photodiodes; and 3. how to further enhance the compatibility of $\chi^{(2)}$ and $\chi^{(3)}$ integrated platforms with other material platforms such as semiconducting or superconducting materials that would bring further advantages.

We believe that a wide adoption of integrated terahertz technologies will stem from two future developments: 1. miniaturization as a driver for optimized operation of custom-cut detectors and emitters; and 2. their further integration into systems that uniquely depend either on small form factors and/or on high-density packaging of entire circuits that are simply unaccessible in bulk optical systems. While the former would allow to minimize the terahertz loss on-chip, increase the maximal bandwidth, and ensure the delivery of maximal power from a source to a detector, thereby enabling a power-efficient chip, the latter would—by mere merit of dimensionality—benefit the many applications that require compactness and an ultra-low price per piece without exception: consumer electronics, the internet of things, communications, and remote sensing.

We showcase in Fig. 4(a) the component-level milestones we deem most central toward the realization of future hybrid terahertz-optical systems. Integrated sources could bypass the need for bulky lasers provided they could co-exist in-line with terahertz emitters and detectors similar to the ones highlighted in the previous sections. Integrated pulse generators (pulsed sources) could enable on-chip electro-optic sampling and broadband terahertz field generation. Going one step further, integrated photodetectors would be very handy for a fast and compact read-out of the up-converted optical light. This would bypass the need for out-of-chip coupling, which typically introduces significant optical loss. For all applications requiring femtosecond pulses, in-line compressors will need to counteract the built-in dispersion in a customized way across the various parts of the chip, e.g., through low-loss waveguides with engineered group velocity dispersion. Finally, on-chip terahertz waveguides could distribute terahertz signals on-chip to the optical components that need them.

Closing the loop, we look back at the big areas of interest for terahertz science displayed in Fig. 1. Clearly, these component-level developments will benefit all areas. In Fig. 4(b), we showcase exemplarily a few use cases. In the area of terahertz wireless communication, integration of the continuous wave sources on the same chip as the optical-to-terahertz transducers and, in parallel, integration of the optical amplifiers and the photodetectors together with the terahertz-to-optical converters are the main steps toward compact, low-cost, and high-speed wireless links.[117] In the area of broadband terahertz spectroscopy, integrated pulsed sources may be explored for the generation of broadband terahertz light from the tip of a waveguide and its further detection after interaction with a specimen. Furthermore, the scalability of integrated circuits from a single-pixel detector to a multi-pixel detector could open applications in coherent hyperspectral imaging. However, many daunting challenges need to be solved beyond the already difficult task of scalability. For example, optical amplifiers on-chip appear essential in this case to ensure sufficient terahertz power per pixel.

Encouraging is the fact that hybrid/heterogeneous integration has been a clear priority in the field of photonics,[118] and several integration efforts are worth mentioning as they could benefit the terahertz equally well. Hybrid integration, i.e., bringing two or several devices from different material platforms into a single package (via transfer printing, photonic wire-bonding, or flip-chip techniques), has provided the possibility of integrating sources, amplifiers, and detectors on silicon or lithium niobate chips.[56,99,119–124] Hybrid integration is appealing for lab-scale and pilot-scale manufacturing; however, its challenging alignment and assembly hinder its implementation for mass production. Instead, heterogeneous integration, i.e., combining various materials into a single chip (via direct growth, deposition, or wafer/die bonding), is highly suited for mass manufacturing in foundries. Several high-performance devices have been reported via heterogeneous integration,[57,125–128] mainly for silicon photonics, including a recently reported fully integrated 800 Gbps silicon photonics transmitter with eight heterogeneously integrated distributed feedback lasers.[129] Although heterogeneous integration is potentially highly attractive for high-volume production, its ultra-clean interface requirement and high-cost fabrication make it challenging on the research lab-scale at the moment.

VI. CONCLUSIONS

Terahertz integrated photonics based on $\chi^{(2)}$ and $\chi^{(3)}$ nonlinearities and photoconduction is, at present, an exciting and rapidly evolving young field. The simplicity of most designs discussed here is a potential advantage for the near-term adoption of integrated

terahertz-optical chips; already, the combination of simple nonlinear waveguides with terahertz antennas enables relatively profound measurement schemes or custom-tailored terahertz radiation. In the long-term, we foresee that important questions will revolve around interfacing these simple building blocks with further photonic structures, as shown in Fig. 4, and revealing the limits in terms of power, linewidth, bandwidth, tunability, and dynamic control of the system as a whole.

On a final note, miniaturization has also been pursued with increasing success in detectors and emitters that operate based on principles not covered in this article, such as intersubband transitions in semiconductor heterostructures (e.g., quantum cascade lasers have been recently integrated into a polymer waveguide platform[130,132]) or the inverse spin-Hall effect (spintronic emitters have been patterned on the tip of an optical fiber[133]). Altogether, these research efforts signal a broad interest in compact, robust, and scalable hybrid optical-terahertz chips.

ACKNOWLEDGMENTS

S.R. and I.-C.B.-C. acknowledge funding from the Swiss National Science Foundation under PRIMA Grant No. 201547.

AUTHOR DECLARATIONS

Conflict of Interest

The authors have no conflicts to disclose.

Author Contributions

S.R. and I.-C.B.-C. contributed equally to this work.

Shima Rajabali: Conceptualization (equal); Formal analysis (equal); Methodology (equal); Visualization (equal); Writing – original draft (equal); Writing – review & editing (equal). **Ileana-Cristina Benea-Chelmus**: Conceptualization (equal); Funding acquisition (lead); Investigation (lead); Methodology (equal); Project administration (lead); Supervision (lead); Validation (equal); Writing – original draft (equal); Writing – review & editing (equal).

DATA AVAILABILITY

The data that support the findings of this study are available from the corresponding author upon reasonable request.

REFERENCES

[1]T. Tetsumoto, T. Nagatsuma, M. E. Fermann, G. Navickaite, M. Geiselmann, and A. Rolland, "Optically referenced 300 GHz millimetre-wave oscillator," Nat. Photonics **15**, 516–522 (2021).
[2]D. M. Mittleman, "Twenty years of terahertz imaging [Invited]," Opt. Express **26**, 9417–9431 (2018).
[3]K. Ahi, N. Asadizanjani, S. Shahbazmohamadi, M. Tehranipoor, and M. Anwar, "Terahertz characterization of electronic components and comparison of terahertz imaging with x-ray imaging techniques," Proc. SPIE **9483**, 94830K (2015).
[4]J. B. Perraud, A. F. Obaton, J. Bou-Sleiman, B. Recur, H. Balacey, F. Darracq, J. P. Guillet, and P. Mounaix, "Terahertz imaging and tomography as efficient instruments for testing polymer additive manufacturing objects," Appl. Opt. **55**, 3462–3467 (2016).
[5]M. E. Khani, Z. B. Harris, O. B. Osman, A. J. Singer, and M. Hassan Arbab, "Triage of *in vivo* burn injuries and prediction of wound healing outcome using neural networks and modeling of the terahertz permittivity based on the double Debye dielectric parameters," Biomed. Opt. Express **14**, 918–931 (2023).
[6]L. Luo, L. Men, Z. Liu, Y. Mudryk, X. Zhao, Y. Yao, J. M. Park, R. Shinar, J. Shinar, K.-M. Ho, I. E. Perakis, J. Vela, and J. Wang, "Ultrafast terahertz snapshots of excitonic Rydberg states and electronic coherence in an organometal halide perovskite," Nat. Commun. **8**, 15565 (2017).
[7]C. G. Wade, M. Marcuzzi, E. Levi, J. M. Kondo, I. Lesanovsky, C. S. Adams, and K. J. Weatherill, "A terahertz-driven non-equilibrium phase transition in a room temperature atomic vapour," Nat. Commun. **9**, 3567 (2018).
[8]L. A. Downes, A. R. MacKellar, D. J. Whiting, C. Bourgenot, C. S. Adams, and K. J. Weatherill, "Full-field terahertz imaging at kilohertz frame rates using atomic vapor," Phys. Rev. X **10**, 011027 (2020).
[9]L. Rezac, P. Hartogh, R. Güsten, H. Wiesemeyer, H. W. Hübers, C. Jarchow, H. Richter, B. Klein, and N. Honingh, "First detection of the 63 μm atomic oxygen line in the thermosphere of Mars with GREAT/SOFIA," Astron. Astrophys. **580**, L10 (2015).
[10]S. Heyminck, U. U. Graf, R. Güsten, J. Stutzki, H. W. Hübers, and P. Hartogh, "GREAT: The SOFIA high-frequency heterodyne instrument," Astron. Astrophys. **542**, L1 (2012).
[11]Autonomous car icon, https://www.seekpng.com/ima/u2e6a9u2q8e6y3a9/; accessed February 2023.
[12]Smart watch icon, https://icon-library.com/icon/smart-watch-icon-21.html; accessed February 2023.
[13]Microscope icon, https://www.vecteezy.com/vector-art/2564912-covid19-particle-in-microscope-and-dna-molecule-flat-style-icon; accessed February 2023.
[14]qcomputing icon, https://www.flaticon.com/free-icon/quantum-computing_9423138; accessed February 2023.
[15]Satellite icon, https://www.flaticon.com/free-icon/satellite_1062195; accessed February 2023.
[16]Imaging icon, https://pngtree.com/freepng/hand-x-ray-flat-multi-color-icon_3777213.html; accessed February 2023.
[17]A. L. Gaeta, M. Lipson, and T. J. Kippenberg, "Photonic-chip-based frequency combs," Nat. Photonics **13**, 158–169 (2019).
[18]J. Liu, E. Lucas, A. S. Raja, J. He, J. Riemensberger, R. N. Wang, M. Karpov, H. Guo, R. Bouchand, and T. J. Kippenberg, "Photonic microwave generation in the X- and K-band using integrated soliton microcombs," Nat. Photonics **14**, 486–491 (2020).
[19]M. Zhang, B. Buscaino, C. Wang, A. Shams-Ansari, C. Reimer, R. Zhu, J. M. Kahn, and M. Lončar, "Broadband electro-optic frequency comb generation in a lithium niobate microring resonator," Nature **568**, 373–377 (2019).
[20]B. J. Shastri, A. N. Tait, T. Ferreira de Lima, W. H. P. Pernice, H. Bhaskaran, C. D. Wright, and P. R. Prucnal, "Photonics for artificial intelligence and neuromorphic computing," Nat. Photonics **15**, 102–114 (2021).
[21]B. Bai, Q. Yang, H. Shu, L. Chang, F. Yang, B. Shen, Z. Tao, J. Wang, S. Xu, W. Xie, W. Zou, W. Hu, J. E. Bowers, and X. Wang, "Microcomb-based integrated photonic processing unit," Nat. Commun. **14**, 66 (2023).
[22]G. Scalari, J. Faist, and N. Picqué, "On-chip mid-infrared and THz frequency combs for spectroscopy," Appl. Phys. Lett. **114**, 150401 (2019).
[23]A. Shams-Ansari, M. Yu, Z. Chen, C. Reimer, M. Zhang, N. Picqué, and M. Lončar, "Thin-film lithium-niobate electro-optic platform for spectrally tailored dual-comb spectroscopy," Commun. Phys. **5**, 88 (2022).
[24]G. Moody, V. J. Sorger, D. J. Blumenthal, P. W. Juodawlkis, W. Loh, C. Sorace-Agaskar, A. E. Jones, K. C. Balram, J. C. F. Matthews, A. Laing, M. Davanco, L. Chang, J. E. Bowers, N. Quack, C. Galland, I. Aharonovich, M. A. Wolff, C. Schuck, N. Sinclair, M. Lončar, T. Komljenovic, D. Weld, S. Mookherjea, S. Buckley, M. Radulaski, S. Reitzenstein, B. Pingault, B. Machielse, D. Mukhopadhyay, A. Akimov, A. Zheltikov, G. S. Agarwal, K. Srinivasan, J. Lu, H. X. Tang, W. Jiang, T. P. McKenna, A. H. Safavi-Naeini, S. Steinhauer, A. W. Elshaari, V. Zwiller, P. S. Davids, N. Martinez, M. Gehl, J. Chiaverini, K. K. Mehta, J. Romero, N. B.

Lingaraju, A. M. Weiner, D. Peace, R. Cernansky, M. Lobino, E. Diamanti, L. T. Vidarte, and R. M. Camacho, "2022 Roadmap on integrated quantum photonics," J. Phys.: Photonics **4**, 012501 (2022).
[25]S. Slussarenko and G. J. Pryde, "Photonic quantum information processing: A concise review," Appl. Phys. Rev. **6**, 041303 (2019).
[26]J. W. Silverstone, D. Bonneau, J. L. O'Brien, and M. G. Thompson, "Silicon quantum photonics," IEEE J. Sel. Top. Quantum Electron. **22**, 390–402 (2016).
[27]M. Sakib, R. Kumar, C. Ma, D. Huang, X. Wu, G.-L. Su, and H. Rong, "A 240 Gb/s PAM4 silicon micro-ring optical modulator," in *Optical Fiber Communication Conference (OFC) 2022* (Optica Publishing Group, 2022), p. M2D.4.
[28]P. Kharel, C. Reimer, K. Luke, L. He, and M. Zhang, "Breaking voltage-bandwidth limits in integrated lithium niobate modulators using micro-structured electrodes: Erratum," Optica **8**, 1218 (2021).
[29]Y. Hu, M. Yu, B. Buscaino, N. Sinclair, D. Zhu, R. Cheng, A. Shams-Ansari, L. Shao, M. Zhang, J. M. Kahn, and M. Lončar, "High-efficiency and broadband on-chip electro-optic frequency comb generators," Nat. Photonics **16**(10), 679–685 (2022).
[30]J. Li and K. Vahala, "Small-sized, ultra-low phase noise photonic microwave oscillators at X-Ka bands," Optica **10**, 33–34 (2023).
[31]A. Tikan, A. Tusnin, J. Riemensberger, M. Churaev, X. Ji, K. N. Komagata, R. N. Wang, J. Liu, and T. J. Kippenberg, "Protected generation of dissipative Kerr solitons in supermodes of coupled optical microresonators," Sci. Adv. **8**, 13 (2022).
[32]Ó. B. Helgason, F. R. Arteaga-Sierra, Z. Ye, K. Twayana, P. A. Andrekson, M. Karlsson, J. Schröder, and V. Torres-Company, "Dissipative solitons in photonic molecules," Nat. Photonics **15**, 305–310 (2021).
[33]M. Zhang, C. Wang, Y. Hu, A. Shams-Ansari, T. Ren, S. Fan, and M. Lončar, "Electronically programmable photonic molecule," Nat. Photonics **13**, 36–40 (2019).
[34]A. Stockklauser, P. Scarlino, J. V. Koski, S. Gasparinetti, C. K. Andersen, C. Reichl, W. Wegscheider, T. Ihn, K. Ensslin, and A. Wallraff, "Strong coupling cavity QED with gate-defined double quantum dots enabled by a high impedance resonator," Phys. Rev. X **7**, 011030 (2017).
[35]Z. L. Newman, V. Maurice, T. Drake, J. R. Stone, T. C. Briles, D. T. Spencer, C. Fredrick, Q. Li, D. Westly, B. R. Ilic, B. Shen, M.-G. Suh, K. Y. Yang, C. Johnson, D. M. S. Johnson, L. Hollberg, K. J. Vahala, K. Srinivasan, S. A. Diddams, J. Kitching, S. B. Papp, and M. T. Hummon, "Architecture for the photonic integration of an optical atomic clock," Optica **6**, 680–685 (2019).
[36]S. B. Papp, K. Beha, P. Del'Haye, F. Quinlan, H. Lee, K. J. Vahala, and S. A. Diddams, "Microresonator frequency comb optical clock," Optica **1**, 10–14 (2014).
[37]J.-C. Besse, K. Reuer, M. C. Collodo, A. Wulff, L. Wernli, A. Copetudo, D. Malz, P. Magnard, A. Akin, M. Gabureac, G. J. Norris, J. I. Cirac, A. Wallraff, and C. Eichler, "Realizing a deterministic source of multipartite-entangled photonic qubits," Nat. Commun. **11**, 4877 (2020).
[38]A. J. Metcalf, C. D. Fredrick, R. C. Terrien, S. B. Papp, and S. A. Diddams, "30 GHz electro-optic frequency comb spanning 300 THz in the near infrared and visible," Opt. Lett. **44**, 2673–2676 (2019).
[39]J. Fatome, I. El-Mansouri, J.-L. Blanchet, S. Pitois, G. Millot, S. Trillo, and S. Wabnitz, "Even harmonic pulse train generation by cross-polarization-modulation seeded instability in optical fibers," J. Opt. Soc. Am. B **30**, 99–106 (2013).
[40]T. Nagatsuma, G. Ducournau, and C. C. Renaud, "Advances in terahertz communications accelerated by photonics," Nat. Photonics **10**, 371–379 (2016).
[41]A. Schneider, M. Neis, M. Stillhart, B. Ruiz, R. U. A. Khan, and P. Günter, "Generation of terahertz pulses through optical rectification in organic DAST crystals: Theory and experiment," J. Opt. Soc. Am. B **23**, 1822 (2006).
[42]Y. Lee, *Principles of Terahertz Science and Technology*, *Lecture Notes in Physics* (Springer US, 2009).
[43]S. Zhang, J. M. Silver, X. Shang, L. Del Bino, N. M. Ridler, and P. Del'Haye, "Terahertz wave generation using a soliton microcomb," Opt. Express **27**, 35257–35266 (2019).
[44]B. Wang, J. S. Morgan, K. Sun, M. Jahanbozorgi, Z. Yang, M. Woodson, S. Estrella, A. Beling, and X. Yi, "Towards high-power, high-coherence, integrated photonic mmWave platform with microcavity solitons," Light: Sci. Appl. **10**, 4 (2021).
[45]W. Wang, P.-K. Lu, A. K. Vinod, D. Turan, J. F. McMillan, H. Liu, M. Yu, D.-L. Kwong, M. Jarrahi, and C. W. Wong, "Coherent terahertz radiation with 2.8-octave tunability through chip-scale photomixed microresonator optical parametric oscillation," Nat. Commun. **13**, 5123 (2022).
[46]T. Göbel, D. Stanze, B. Globisch, R. J. B. Dietz, H. Roehle, and M. Schell, "Telecom technology based continuous wave terahertz photomixing system with 105 decibel signal-to-noise ratio and 35 terahertz bandwidth," Opt. Lett. **38**, 4197–4199 (2013).
[47]A. Deninger, "11—State-of-the-art in terahertz continuous-wave photomixer systems," in *Handbook of Terahertz Technology for Imaging, Sensing and Communications*, *Woodhead Publishing Series in Electronic and Optical Materials*, edited by D. Saeedkia (Woodhead Publishing, 2013), pp. 327–373.
[48]P. Chen, M. Hosseini, and A. Babakhani, "An integrated germanium-based optical waveguide coupled THz photoconductive antenna in silicon," in *Conference on Lasers and Electro-Optics* (Optica Publishing Group, 2016), p. STh3I.2.
[49]J. P. Seddon, M. Natrella, X. Lin, C. Graham, C. C. Renaud, and A. J. Seeds, "Photodiodes for terahertz applications," IEEE J. Sel. Top. Quantum Electron. **28**, 3801612 (2022).
[50]I. D. Henning, M. J. Adams, Y. Sun, D. G. Moodie, D. C. Rogers, P. J. Cannard, S. J. Dosanjh, M. Skuse, and R. J. Firth, "Broadband antenna-integrated, edge-coupled photomixers for tuneable terahertz sources," IEEE J. Quantum Electron. **46**, 1498–1505 (2010).
[51]UTC-photomixer module, https://www.ntt-electronics.com/en/sensing_application/thz_products.html\#utc-pd; accessed July 2023.
[52]H. Page, S. Malik, M. Evans, I. Gregory, I. Farrer, and D. Ritchie, "Waveguide coupled terahertz photoconductive antennas: Toward integrated photonic terahertz devices," Appl. Phys. Lett. **92**, 163502 (2008).
[53]L. Consolino, A. Taschin, P. Bartolini, S. Bartalini, P. Cancio, A. Tredicucci, H. E. Beere, D. A. Ritchie, R. Torre, M. S. Vitiello, and P. De Natale, "Phase-locking to a free-space terahertz comb for metrological-grade terahertz lasers," Nat. Commun. **3**, 1040 (2012).
[54]A. Herter, A. Shams-Ansari, F. F. Settembrini, H. K. Warner, J. Faist, M. Lončar, and I.-C. Benea-Chelmus, "Terahertz waveform synthesis in integrated thin-film lithium niobate platform," Nat. Commun. **14**, 11 (2023).
[55]N. Kuse, K. Nishimoto, Y. Tokizane, S. Okada, G. Navickaite, M. Geiselmann, K. Minoshima, and T. Yasui, "Low phase noise THz generation from a fiber-referenced Kerr microresonator soliton comb," Commun. Phys. **5**, 312 (2022).
[56]X. Guo, L. Shao, L. He, K. Luke, J. Morgan, K. Sun, J. Gao, T.-C. Tzu, Y. Shen, D. Chen, B. Guo, F. Yu, Q. Yu, M. Jafari, M. Lončar, M. Zhang, and A. Beling, "High-performance modified uni-traveling carrier photodiode integrated on a thin-film lithium niobate platform," Photonics Res. **10**, 1338–1343 (2022).
[57]S. Lischke, A. Peczek, J. S. Morgan, K. Sun, D. Steckler, Y. Yamamoto, F. Korndörfer, C. Mai, S. Marschmeyer, M. Fraschke, A. Krüger, A. Beling, and L. Zimmermann, "Ultra-fast germanium photodiode with 3-dB bandwidth of 265 GHz," Nat. Photonics **15**, 925–931 (2021).
[58]P. Ma, Y. Salamin, B. Baeuerle, A. Josten, W. Heni, A. Emboras, and J. Leuthold, "Plasmonically enhanced graphene photodetector featuring 100 Gbit/s data reception, high responsivity, and compact size," ACS Photonics **6**, 154–161 (2019).
[59]S. Nellen, T. Ishibashi, A. Deninger, R. B. Kohlhaas, L. Liebermeister, M. Schell, and B. Globisch, "Experimental comparison of UTC- and PIN-photodiodes for continuous-wave terahertz generation," J. Infrared, Millimeter, Terahertz Waves **41**, 343–354 (2020).
[60]E. Peytavit, S. Lepilliet, F. Hindle, C. Coinon, T. Akalin, G. Ducournau, G. Mouret, and J.-F. Lampin, "Milliwatt-level output power in the sub-terahertz range generated by photomixing in a GaAs photoconductor," Appl. Phys. Lett. **99**, 223508 (2011).
[61]S. Nellen, S. Lauck, E. Peytavit, P. Szriftgiser, M. Schell, G. Ducournau, and B. Globisch, "Coherent wireless link at 300 GHz with 160 Gbit/s enabled by a photonic transmitter," J. Lightwave Technol. **40**, 4178–4185 (2022).
[62]P. Chen, M. Hosseini, and A. Babakhani, "An integrated germanium-based THz impulse radiator with an optical waveguide coupled photoconductive switch in silicon," Micromachines **10**, 367 (2019).

[63]Y. Salamin, I.-C. Benea-Chelmus, Y. Fedoryshyn, W. Heni, D. L. Elder, L. R. Dalton, J. Faist, and J. Leuthold, "Compact and ultra-efficient broadband plasmonic terahertz field detector," Nat. Commun. **10**, 5550 (2019).
[64]E. Castro-Camus, L. Fu, J. Lloyd-Hughes, H. H. Tan, C. Jagadish, and M. B. Johnston, "Photoconductive response correction for detectors of terahertz radiation," J. Appl. Phys. **104**, 053113 (2008).
[65]I.-C. Benea-Chelmus, Y. Salamin, F. F. Settembrini, Y. Fedoryshyn, W. Heni, D. L. Elder, L. R. Dalton, J. Leuthold, and J. Faist, "Electro-optic interface for ultrasensitive intracavity electric field measurements at microwave and terahertz frequencies," Optica **7**, 498 (2020).
[66]M. Deumer, S. Nellen, S. Breuer, R. B. Kohlhaas, L. Schwenson, K. Wenzel, L. Liebermeister, M. Schell, and B. Globisch, "Waveguide-integrated photoconductive THz receivers," in *2022 47th International Conference on Infrared, Millimeter and Terahertz Waves (IRMMW-THz)* (IEEE, 2022), pp. 1–2.
[67]H. Zwickel, S. Singer, C. Kieninger, Y. Kutuvantavida, N. Muradyan, T. Wahlbrink, S. Yokoyama, S. Randel, W. Freude, and C. Koos, "Verified equivalent-circuit model for slot-waveguide modulators," Opt. Express **28**, 12951–12976 (2020).
[68]A. Schwarzenberger, A. Kuzmin, C. Eschenbaum, C. Füllner, A. Mertens, L. Johnson, D. L. Elder, S. R. Hammond, L. Dalton, S. Randel, W. Freude, and C. Koos, "Cryogenic operation of a silicon-organic hybrid (SOH) modulator at 50 Gbit/s and 4 K ambient temperature," in *European Conference on Optical Communication (ECOC) 2022* (Optica Publishing Group, 2022), p. Th3B.3.
[69]M. H. P. Pfeiffer, A. Kordts, V. Brasch, M. Zervas, M. Geiselmann, J. D. Jost, and T. J. Kippenberg, "Photonic Damascene process for integrated high-Q microresonator based nonlinear photonics," Optica **3**, 20–25 (2016).
[70]D. J. Blumenthal, R. Heideman, D. Geuzebroek, A. Leinse, and C. Roeloffzen, "Silicon nitride in silicon photonics," Proc. IEEE **106**, 2209–2231 (2018).
[71]J. Dai, J. Zhang, W. Zhang, and D. Grischkowsky, "Terahertz time-domain spectroscopy characterization of the far-infrared absorption and index of refraction of high-resistivity, float-zone silicon," J. Opt. Soc. Am. B **21**, 1379–1386 (2004).
[72]X. Wu, C. Zhou, W. R. Huang, F. Ahr, and F. X. Kärtner, "Temperature dependent refractive index and absorption coefficient of congruent lithium niobate crystals in the terahertz range," Opt. Express **23**, 29729–29737 (2015).
[73]M. Unferdorben, Z. Szaller, I. Hajdara, J. Hebling, and L. Pálfalvi, "Measurement of refractive index and absorption coefficient of congruent and stoichiometric lithium niobate in the terahertz range," J. Infrared, Millimeter, Terahertz Waves **36**, 1203–1209 (2015).
[74]S.-J. Kim, B. J. Kang, U. Puc, W. T. Kim, M. Jazbinsek, F. Rotermund, and O.-P. Kwon, "Highly nonlinear optical organic crystals for efficient terahertz wave generation, detection, and applications," Adv. Opt. Mater. **9**, 2101019 (2021).
[75]H. Bao, K. Nielsen, O. Bang, and P. U. Jepsen, "Dielectric tube waveguides with absorptive cladding for broadband, low-dispersion and low loss THz guiding," Sci. Rep. **5**, 7620 (2015).
[76]H. Xu, F. Liu, D. L. Elder, L. E. Johnson, Y. de Coene, K. Clays, B. H. Robinson, and L. R. Dalton, "Ultrahigh electro-optic coefficients, high index of refraction, and long-term stability from Diels–Alder cross-linkable binary molecular glasses," Chem. Mater. **32**, 1408–1421 (2020).
[77]A. Abohmra, H. Abbas, M. Al-Hasan, I. B. Mabrouk, A. Alomainy, M. A. Imran, and Q. H. Abbasi, "Terahertz antenna array based on a hybrid perovskite structure," IEEE Open J. Antennas Propag. **1**, 464–471 (2020).
[78]R. Singh, A. Azad, and W. Zhang, "9—Resonant field enhancement of terahertz waves in subwavelength plasmonic structures," in *Handbook of Terahertz Technology for Imaging, Sensing and Communications*, *Series in Electronic and Optical Materials* (Woodhead Publishing, 2013), pp. 272–294.
[79]N. Laman and D. Grischkowsky, "Terahertz conductivity of thin metal films," Appl. Phys. Lett. **93**, 051105 (2008).
[80]Y. He, Y. Chen, L. Zhang, S.-W. Wong, and Z. N. Chen, "An overview of terahertz antennas," China Commun. **17**, 124–165 (2020).
[81]S. Dash and A. Patnaik, "Material selection for THz antennas," Microwave Opt. Technol. Lett. **60**, 1183–1187 (2018).
[82]W. Withayachumnankul, R. Yamada, C. Fumeaux, M. Fujita, and T. Nagatsuma, "All-dielectric integration of dielectric resonator antenna and photonic crystal waveguide," Opt. Express **25**, 14706–14714 (2017).
[83]A. Karamlou, M. E. Trusheim, and D. Englund, "Metal-dielectric antennas for efficient photon collection from diamond color centers," Opt. Express **26**, 3341–3352 (2018).
[84]T. Saeidi, I. Ismail, A. R. H. Alhawari, A. Sali, and A. Ismail, "High gain dual-band couple feed transparent THz antenna for satellite communications," in *2016 IEEE Asia-Pacific Conference on Applied Electromagnetics (APACE)* (IEEE, 2016), pp. 11–15.
[85]Z. Xu, X. Dong, and J. Bornemann, "Design of a reconfigurable mimo system for THz communications based on graphene antennas," IEEE Trans. Terahertz Sci. Technol. **4**, 609–617 (2014).
[86]A. E. Yachmenev, D. V. Lavrukhin, I. A. Glinskiy, N. V. Zenchenko, Y. G. Goncharov, I. E. Spektor, R. A. Khabibullin, T. Otsuji, and D. S. Ponomarev, "Metallic and dielectric metasurfaces in photoconductive terahertz devices: A review," Opt. Eng. **59**, 061608 (2019).
[87]D. E. Zelmon, D. L. Small, and D. Jundt, "Infrared corrected Sellmeier coefficients for congruently grown lithium niobate and 5 mol% magnesium oxide-doped lithium niobate," J. Opt. Soc. Am. B **14**, 3319–3322 (1997).
[88]I.-C. Benea-Chelmus, M. L. Meretska, D. L. Elder, M. Tamagnone, L. R. Dalton, and F. Capasso, "Electro-optic spatial light modulator from an engineered organic layer," Nat. Commun. **12**, 5928 (2021).
[89]Y. Takahashi, H. Adachi, T. Taniuchi, M. Takagi, Y. Hosokawa, S. Onzuka, S. Brahadeeswaran, M. Yoshimura, Y. Mori, H. Masuhara, T. Sasaki, and H. Nakanishi, "Organic nonlinear optical DAST crystals for electro-optic measurement and terahertz wave generation," J. Photochem. Photobiol., A **183**, 247–252 (2006), part of Special Issue: Proceedings of 12th International Conference on Unconventional Photoactive Systems (UPS-12).
[90]H. Uchida, T. Kawauchi, G. Otake, C. Koyama, K. Takeya, and S. R. Tripathi, "Optical thin film coated organic nonlinear crystal for efficient terahertz wave generation," Sci. Rep. **12**, 15082 (2022).
[91]L. Mutter, F. D. Brunner, Z. Yang, M. Jazbinšek, and P. Günter, "Linear and nonlinear optical properties of the organic crystal DSTMS," J. Opt. Soc. Am. B **24**, 2556–2561 (2007).
[92]Z. Yang, L. Mutter, M. Stillhart, B. Ruiz, S. Aravazhi, M. Jazbinsek, A. Schneider, V. Gramlich, and P. Günter, "Large-size bulk and thin-film stilbazolium-salt single crystals for nonlinear optics and THz generation," Adv. Funct. Mater. **17**, 2018–2023 (2007).
[93]K. Luke, Y. Okawachi, M. R. E. Lamont, A. L. Gaeta, and M. Lipson, "Broadband mid-infrared frequency comb generation in a Si_3N_4 microresonator," Opt. Lett. **40**, 4823–4826 (2015).
[94]D. Zhu, L. Shao, M. Yu, R. Cheng, B. Desiatov, C. J. Xin, Y. Hu, J. Holzgrafe, S. Ghosh, A. Shams-Ansari, E. Puma, N. Sinclair, C. Reimer, M. Zhang, and M. Lončar, "Integrated photonics on thin-film lithium niobate," Adv. Opt. Photonics **13**, 242–352 (2021).
[95]J. Lu, J. B. Surya, X. Liu, Y. Xu, and H. X. Tang, "Octave-spanning supercontinuum generation in nanoscale lithium niobate waveguides," Opt. Lett. **44**, 1492–1495 (2019).
[96]D. D. Hickstein, H. Jung, D. R. Carlson, A. Lind, I. Coddington, K. Srinivasan, G. G. Ycas, D. C. Cole, A. Kowligy, C. Fredrick, S. Droste, E. S. Lamb, N. R. Newbury, H. X. Tang, S. A. Diddams, and S. B. Papp, "Ultrabroadband supercontinuum generation and frequency-comb stabilization using on-chip waveguides with both cubic and quadratic nonlinearities," Phys. Rev. Appl. **8**, 014025 (2017).
[97]T. Herr, V. Brasch, J. D. Jost, I. Mirgorodskiy, G. Lihachev, M. L. Gorodetsky, and T. J. Kippenberg, "Mode spectrum and temporal soliton formation in optical microresonators," Phys. Rev. Lett. **113**, 123901 (2014).
[98]M. H. Anderson, W. Weng, G. Lihachev, A. Tikan, J. Liu, and T. J. Kippenberg, "Zero dispersion Kerr solitons in optical microresonators," Nat. Commun. **13**, 4764 (2022).
[99]M. Yu, D. Barton III, R. Cheng, C. Reimer, P. Kharel, L. He, L. Shao, D. Zhu, Y. Hu, H. R. Grant, L. Johansson, Y. Okawachi, A. L. Gaeta, M. Zhang, and M. Lončar, "Integrated femtosecond pulse generator on thin-film lithium niobate," Nature **612**, 252–258 (2022).
[100]D. T. F. Marple, "Refractive index of ZnSe, ZnTe, and CdTe," J. Appl. Phys. **35**, 539–542 (1964).

[101]H. P. Wagner, M. Kühnelt, W. Langbein, and J. M. Hvam, "Dispersion of the second-order nonlinear susceptibility in ZnTe, ZnSe, and ZnS," Phys. Rev. B **58**, 10494–10501 (1998).
[102]B. Pradarutti, G. Matthäus, S. Riehemann, G. Notni, S. Nolte, and A. Tünnermann, "Highly efficient terahertz electro-optic sampling by material optimization at 1060 nm," Opt. Commun. **281**, 5031–5035 (2008).
[103]W.-Q. He, C.-M. Gu, and W.-Z. Shen, "Direct evidence of Kerr-like nonlinearity by femtosecond Z-scan technique," Opt. Express **14**, 5476–5483 (2006).
[104]W. L. Bond, "Measurement of the refractive indices of several crystals," J. Appl. Phys. **36**, 1674–1677 (1965).
[105]Y. Berozashvili, S. Machavariani, A. Natsvlishvili, and A. Chirakadze, "Dispersion of the linear electro-optic coefficients and the non-linear susceptibility in gap," J. Phys. D: Appl. Phys. **22**, 682 (1989).
[106]I. Shoji, T. Kondo, A. Kitamoto, M. Shirane, and R. Ito, "Absolute scale of second-order nonlinear-optical coefficients," J. Opt. Soc. Am. B **14**, 2268–2294 (1997).
[107]F. Liu, Y. Li, Q. Xing, L. Chai, M. Hu, C. Wang, Y. Deng, Q. Sun, and C. Wang, "Three-photon absorption and Kerr nonlinearity in undoped bulk gap excited by a femtosecond laser at 1040 nm," J. Opt. **12**, 095201 (2010).
[108]R. S. Weis and T. K. Gaylord, "Lithium niobate: Summary of physical properties and crystal structure," Appl. Phys. A: Solids Surf. **37**, 191–203 (1985).
[109]C. Kieninger, Y. Kutuvantavida, D. L. Elder, S. Wolf, H. Zwickel, M. Blaicher, J. N. Kemal, M. Lauermann, S. Randel, W. Freude, L. R. Dalton, and C. Koos, "Ultra-high electro-optic activity demonstrated in a silicon-organic hybrid modulator," Optica **5**, 739–748 (2018).
[110]F. Pan, G. Knöpfle, C. Bosshard, S. Follonier, R. Spreiter, M. Wong, and P. Günter, "Electro-optic properties of the organic salt 4-N,N-dimethylamino-4-N-methyl-stilbazolium tosylate," Appl. Phys. Lett. **69**, 13–15 (1996).
[111]U. Meier, M. Bösch, C. Bosshard, F. Pan, and P. Günter, "Parametric interactions in the organic salt 4-N,N-dimethylamino-4-N-methyl-stilbazolium tosylate at telecommunication wavelengths," J. Appl. Phys. **83**, 3486–3489 (1998).
[112]J. He, H. Chen, J. Hu, J. Zhou, Y. Zhang, A. Kovach, C. Sideris, M. C. Harrison, Y. Zhao, and A. M. Armani, "Nonlinear nanophotonic devices in the ultraviolet to visible wavelength range," Nanophotonics **9**, 3781–3804 (2020).
[113]P. Gräupner, J. C. Pommier, A. Cachard, and J. L. Coutaz, "Electro-optical effect in aluminum nitride waveguides," J. Appl. Phys. **71**, 4136–4139 (1992).
[114]M. Jankowski, C. Langrock, B. Desiatov, A. Marandi, C. Wang, M. Zhang, C. R. Phillips, M. Lončar, and M. M. Fejer, "Ultrabroadband nonlinear optics in nanophotonic periodically poled lithium niobate waveguides," Optica **7**, 40–46 (2020).
[115]C. Wang, C. Langrock, A. Marandi, M. Jankowski, M. Zhang, B. Desiatov, M. M. Fejer, and M. Lončar, "Ultrahigh-efficiency wavelength conversion in nanophotonic periodically poled lithium niobate waveguides," Optica **5**, 1438–1441 (2018).
[116]P. Habegger, Y. Horst, S. M. Koepfli, M. Kohli, E. D. Leo, D. Bisang, M. Destraz, V. Tedaldi, N. Meier, N. D. Medico, W. Wang, C. Hoessbacher, B. Baeuerle, W. Heni, and J. Leuthold, "Plasmonic 100-GHz electro-optic modulators for cryogenic applications," in *European Conference on Optical Communication (ECOC) 2022* (Optica Publishing Group, 2022), p. Tu1G.1.
[117]S. Jia, M.-C. Lo, L. Zhang, O. Ozolins, A. Udalcovs, D. Kong, X. Pang, R. Guzman, X. Yu, S. Xiao, S. Popov, J. Chen, G. Carpintero, T. Morioka, H. Hu, and L. K. Oxenløwe, "Integrated dual-laser photonic chip for high purity carrier generation enabling ultrafast terahertz wireless communications," Nat. Commun. **13**, (2022).
[118]P. Kaur, A. Boes, G. Ren, T. G. Nguyen, G. Roelkens, and A. Mitchell, "Hybrid and heterogeneous photonic integration," APL Photonics **6**, 061102 (2021).
[119]R. Kumar, D. Huang, M. Sakib, G.-L. Su, C. Ma, X. Wu, and H. Rong, "Integrated multi-wavelength DFB laser with 200 GHz channel spacing," Proc. SPIE **12021**, 1202106 (2022).
[120]J. Zhang, G. Muliuk, J. Juvert, S. Kumari, J. Goyvaerts, B. Haq, C. Op de Beeck, B. Kuyken, G. Morthier, D. Van Thourhout, R. Baets, G. Lepage, P. Verheyen, J. Van Campenhout, A. Gocalinska, J. O'Callaghan, E. Pelucchi, K. Thomas, B. Corbett, A. J. Trindade, and G. Roelkens, "III-V-on-Si photonic integrated circuits realized using micro-transfer-printing," APL Photonics **4**, 110803 (2019).
[121]T. Matsumoto, T. Kurahashi, R. Konoike, K. Suzuki, K. Tanizawa, A. Uetake, K. Takabayashi, K. Ikeda, H. Kawashima, S. Akiyama, and S. Sekiguchi, "Hybrid-integration of SOA on silicon photonics platform based on flip-chip bonding," J. Lightwave Technol. **37**, 307–313 (2019).
[122]A. Shams-Ansari, D. Renaud, R. Cheng, L. Shao, L. He, D. Zhu, M. Yu, H. R. Grant, L. Johansson, M. Zhang, and M. Lončar, "Electrically pumped laser transmitter integrated on thin-film lithium niobate," Optica **9**, 408–411 (2022).
[123]N. Lindenmann, G. Balthasar, D. Hillerkuss, R. Schmogrow, M. Jordan, J. Leuthold, W. Freude, and C. Koos, "Photonic wire bonding: a novel concept for chip-scale interconnects," Opt. Express **20**, 17667–17677 (2012).
[124]J. Pfeifle, V. Brasch, M. Lauermann, Y. Yu, D. Wegner, T. Herr, K. Hartinger, P. Schindler, J. Li, D. Hillerkuss, R. Schmogrow, C. Weimann, R. Holzwarth, W. Freude, J. Leuthold, T. J. Kippenberg, and C. Koos, "Coherent terabit communications with microresonator Kerr frequency combs," Nat. Photonics **8**, 375–380 (2014).
[125]Y. Wan, D. Jung, J. Norman, C. Shang, I. MacFarlane, Q. Li, M. J. Kennedy, A. C. Gossard, K. M. Lau, and J. E. Bowers, "O-band electrically injected quantum dot micro-ring lasers on on-axis (001) GaP/Si and V-groove Si," Opt. Express **25**, 26853–26860 (2017).
[126]Y. Xue, Y. Han, Y. Tong, Z. Yan, Y. Wang, Z. Zhang, H. K. Tsang, and K. M. Lau, "High-performance III-V photodetectors on a monolithic InP/SOI platform," Optica **8**, 1204–1209 (2021).
[127]Z. Yan, Y. Han, L. Lin, Y. Xue, C. Ma, W. K. Ng, K. S. Wong, and K. M. Lau, "A monolithic InP/SOI platform for integrated photonics," Light: Sci. Appl. **10**, 200 (2021).
[128]P. Wen, P. Tiwari, S. Mauthe, H. Schmid, M. Sousa, M. Scherrer, M. Baumann, B. I. Bitachon, J. Leuthold, B. Gotsmann, and K. E. Moselund, "Waveguide coupled III-V photodiodes monolithically integrated on Si," Nat. Commun. **13**, 909 (2022).
[129]H. Yu, D. Patel, W. Liu, Y. Malinge, P. Doussiere, W. Lin, S. Gupta, K. Narayanan, I. Hoshino, M. Bresnehan, S. Sunkoju, D. Mantegazza, R. Herrick, R. Venables, H. Mahalingam, P. Seddighian, A. Fuerst, J. Davis, D. Gold, X. Pan, K. Al-hemyari, A. Agrawal, Y. Li, X. Zheng, M. Geethachar, M. Favaro, D. Zhu, A. Liu, and Y. Akulova, "800 Gbps fully integrated silicon photonics transmitter for data center applications," in *2022 Optical Fiber Communications Conference and Exhibition (OFC)* (IEEE, 2022), pp. 1–3.
[130]U. Senica, A. Forrer, T. Olariu, P. Micheletti, S. Cibella, G. Torrioli, M. Beck, J. Faist, and G. Scalari, "Planarized THz quantum cascade lasers for broadband coherent photonics," Light: Sci. Appl. **11**, 347 (2022).
[131]U. Senica, A. Dikopoltsev, A. Forrer, S. Cibella, G. Torrioli, M. Beck, J. Faist, and G. Scalari, "Frequency-modulated combs via on-chip field enhancement," arXiv:2305.01483 [physics.optics] (2023).
[132]P. Micheletti, U. Senica, A. Forrer, S. Cibella, G. Torrioli, M. Frankié, M. Beck, J. Faist, and G. Scalari, "Terahertz optical solitons from dispersion-compensated antenna-coupled planarized ring quantum cascade lasers," Sci. Adv. **9**, (2023).
[133]F. Paries, N. Tiercelin, G. Lezier, M. Vanwolleghem, F. Selz, M.-A. Syskaki, F. Kammerbauer, G. Jakob, M. Jourdan, M. Kläui, Z. Kaspar, T. Kampfrath, T. S. Seifert, G. V. Freymann, and D. Molter, "Fiber-tip spintronic terahertz emitters," arXiv:2305.01365 [physics.optics] (2023).